Nonlinear Thermal Waves:
Part II - Analytical Solutions for Pulses

by

M. S. Cramer
Engineering Science and Mechanics
Virginia Polytechnic Institute and State University
Blacksburg, VA 24061-0219

and

B. B. Lowekamp and L. T. Watson
Department of Computer Science
Virginia Polytechnic Institute and State University
Blacksburg, VA 24061-0106

Abstract

The weak shock theory developed by Cramer (1994) is used to derive explicit solutions for the evolution of one-dimensional weakly nonlinear, weakly relaxing heat pulses in rigid conductors. Formulas and differential equations governing the evolution of general heat inputs are derived and applied to the special cases of a square-wave heat input and a finite width sine-wave heat input. Numerical solutions to the exact Maxwell-Cattaneo theory are also presented and show excellent agreement with these analytical solutions.

1. Introduction

Cramer (1994), hereinafter referred to as Part I, has developed an approximate analytical model for thermal waves which is capable of describing weakly relaxing, weakly nonlinear pulses. The constitutive model was based on the well-known Maxwell-Cattaneo theory which requires that the local heat flux vector $\mathbf{q}$ satisfies the relaxation formula

$$\frac{\partial \mathbf{q}}{\partial t} = -\frac{1}{\tau}\left(\mathbf{q} - \mathbf{q}_{F}\right), \tag{1.1}$$

where t is the time, τ is the thermal relaxation time, and $\mathbf{q}_F$ is the Fourier heat flux. Nonlinearity was introduced through use of temperature-dependent thermal relaxation time, specific heat and thermal conductivity. Although a few specific results were presented, the primary contribution of Part I was to establish the general theory. The purpose of the present investigation is to demonstrate how the results of Part I may be applied to specific heat inputs. In doing so, we will also reveal physical phenomena which are not easily anticipated by an extrapolation of the standard linear theory.

One of the main difficulties in the treatment of nonlinear thermal waves is the interactions between any shock waves which occur and the smooth parts of the thermal wave. The fact that such interactions must always occur is due to the different amplitude dependencies of the speed of smooth waves and of shock waves. As pointed out in Part I, thermal waves immediately behind a shock will always overtake the shock and waves immediately ahead of the shock will always be overtaken by it. Although the weak shock theory described in Part I corresponds to a relatively simple interaction, some effort is required to extract useful formulas. The general interaction formulas and equations will be developed in Section 4 of the present investigation. The results of Section 4 will be valid for most heat inputs encountered in practice.

The general interaction formulas will be applied to specific heat inputs in Sections 5 and 6. The heat inputs chosen are a square-wave heat source and a finite length sinusoidal input. The square wave source corresponds to heater which is switched on at $t = 0$ and then held at a constant heat flux until a time $t = T$ at which time the heater is switched off. This, of course, is one of the simplest waveforms possible and is also one of the easiest to incorporate in an experiment. Because discontinuities in temperature and heat flux are present from the beginning, this example also permits us to address in detail the fate of both admissible and inadmissible discontinuities. Furthermore, the decay of the admissible shock will frequently be enhanced by its interaction with the centered fan arising from the disintegration of the inadmissible discontinuity. Such a shock-centered fan interaction is canonical in the sense that it frequently occurs in many cases of practical interest.

The second heat input described here is smooth in the sense that it contains no discontinuities in the heat input. As a result, the sinusoidal heat source provides a simple illustration of shock formation (provided it occurs) and the subsequent evolution of the shock or shocks. We will also use this example to demonstrate how the relaxation limits the interaction of the shock or shocks with the surrounding disturbance. This contrasts sharply with the undamped nonlinear theory where the shock ultimately is influenced by every portion of the smooth part of the wave. The full details are found in Section 6.

The results presented here are exact solutions to the weak shock theory developed in Part I and summarized in Section 2 of the present article. As pointed out above and in Section 2, this weak shock theory is only an approximation to the exact Maxwell-Cattaneo theory. In order to illustrate the accuracy of the present theory, we will compare the resultant solutions to numerical solutions of the exact Maxwell-Cattaneo theory, i.e., that obtained by combining (1.1) with the energy equation for rigid conductors. The numerical scheme is discussed in more detail in Section 3. The actual comparisons are carried out in Section 5 and 6 where the analytical solutions are presented.

2. Summary of the Weak Shock Theory

In Part I we considered one-dimensional, weakly relaxing thermal pulses of small amplitude in a rigid conductor. The equation governing a right-running finite width pulse was found to be

$$\frac{\partial q}{\partial t} + U_o\left(1 + \Gamma\frac{q}{U_o\rho c_o\theta_o}\right)\frac{\partial q}{\partial x} \approx -\frac{q}{2\tau_o}, \tag{2.1}$$

where x and t are the usual spatial and temporal independent variables, $q = q(x,t)$ is the x component of the instantaneous heat flux, $\theta = \theta(x,t)$ is the absolute temperature, ρ = constant is the mass density of the conductor, $c = c(\theta)$ is the temperature-dependent specific heat of the conductor, $\tau = \tau(\theta)$ is the temperature-dependent thermal relaxation time,

$$U = U(\theta) \equiv \left(\frac{k}{\rho c\tau}\right)^{\frac{1}{2}} \tag{2.2}$$

is the thermal wave speed and

$$\Gamma \equiv \frac{\theta_o U_o'}{U_o} = 0(1) \tag{2.3}$$

is the nondimensional steepening or intrinsic nonlinearity parameter. The prime on U will denote differentiation with respect to temperature and the subscript o will denote quantities evaluated at the undisturbed state which is given by $q = 0$, $\theta = \theta_o$ = constant. The quantity $k = k(\theta)$ is the temperature-dep conductivity. In the weak shock theory of Part I, temperature perturbations were found to be related to q by

$$\frac{\theta - \theta_o}{\theta_o} \approx \frac{q}{U_o\rho c_o\theta_o}. \tag{2.4}$$

The conditions of small amplitude and weak relaxation can be written

$$\epsilon \equiv \frac{q_m}{U_o\rho c_o\theta_o} = 0(\delta) = o(1), \tag{2.5}$$

where

$$\delta \equiv \frac{L}{L_s} = \frac{T}{\tau_o} \tag{2.6}$$

is the thermal decay parameter, L is a measure of the length of the pulse, $T \equiv L/U_o$ is a measure of the duration of the pulse, and $L_s \equiv U_o \tau_o$ is the skin depth or a measure of the propagation distance required for relaxation to damp out the thermal wave. The constant q_m is a measure of the magnitude of the heat flux and ϵ can be thought of as a nondimensional measure of the wave amplitude.

An equivalent form of (2.1) is the method of characteristics solution

$$\frac{dq}{dt} \approx -\frac{q}{2\tau_o} \tag{2.7}$$

on

$$\frac{dx}{dt} \approx U_o \left(1 + \Gamma \frac{q}{U_o \rho c_o \theta_o} \right), \tag{2.8}$$

where the lines defined by (2.8) are referred to as the characteristic lines. A second interpretation of (2.8) is that it is the nonlinear propagation speed of a thermal pulse.

The shock speed, s, corresponding to (2.1) or (2.7)-(2.8) was found to be the average of the nonlinear wave speeds (2.8) and can be written

$$s = U_o \left\{ 1 + \frac{\Gamma}{2} \frac{q_1 + q_2}{U_o \rho c_o \theta_o} \right\} \tag{2.9}$$

where the subscripts 1 and 2 refer to conditions immediately ahead of and immediately behind the thermal shock, respectively. In Part I it was shown that the relation between the jumps in q and θ across the shock is identical to that given by (2.4). Thus, (2.4) can be used throughout the following discussion as the relation between the heat flux and temperature perturbation.

The shock existence conditions stated in Part I required that admissible shocks satisfy

$$\begin{array}{lll} q_2 > q_1 \ , & \theta_2 > \theta_1 \ , & \text{if } \Gamma > 0 \\ q_2 < q_1 \ , & \theta_2 < \theta_1 \ , & \text{if } \Gamma < 0. \end{array} \tag{2.10}$$

That is, only temperature-raising shocks are possible if the steepening parameter (2.3) is positive and only temperature-lowering shocks are possible if $\Gamma < 0$.

In the present paper it is convenient to work with the transformed versions of (2.1) and (2.7)-(2.8) as derived in Part I. These read

$$\frac{\partial u}{\partial \xi} - sgn(\Gamma) u \frac{\partial u}{\partial \chi} = 0, \tag{2.11}$$

or

$$u = \text{constant on } \chi = -sgn(\Gamma) u \xi + \text{constant}, \tag{2.12}$$

where

$$u = u(\xi, \chi) \equiv \frac{q}{q_m} e^{\frac{x}{2L_s}} \tag{2.13}$$

$$\xi = \xi\left(\frac{x}{L_s}\right) \equiv \frac{2\epsilon|\Gamma|}{\delta}\left(1 - e^{-\frac{x}{2L_s}}\right) \tag{2.14}$$

$$\chi = \chi(x, t) \equiv \frac{U_o t - x}{L} \tag{2.15}$$

are the transformed dependent and independent variables. The symbol $sgn(\Gamma)$ denotes the sign of Γ and the two constants in (2.12) are not necessarily the same. The corresponding shock speed can be written in terms of its slope in the $\chi - \xi$ plane as

$$\frac{d\chi_s}{d\xi} = -sgn(\Gamma)\frac{u_1 + u_2}{2}, \tag{2.16}$$

where $\chi = \chi_s(\xi)$ is the shock trajectory in the $\chi - \xi$ plane.

In the following sections we assume that the disturbances are generated by a heat source located at $x = 0$ and defined by

$$q(0,t) \equiv q_m \mathcal{F}\left(\frac{t}{T}\right), \tag{2.17}$$

where $\mathcal{F} = 0$ for $t < 0$ and $t > T$.

3. Numerical Scheme

In Sections 5 and 6 we will compare our analytical solutions to numerical solutions of the exact one-dimensional Maxwell-Cattaneo equations; in dimensional form these equations can be written

$$\rho c \frac{\partial \theta}{\partial t} + \frac{\partial q}{\partial x} = 0$$

$$\frac{\partial q}{\partial t} + \frac{k}{\tau}\frac{\partial \theta}{\partial x} = -\frac{q}{\tau} \ , \tag{3.1}$$

where all parameters have exactly the same definitions as in Section 2. The particular scheme employed is that of Lowekamp, Watson and Cramer (1994); a full description and comparison with known solutions can be found in their article. Alternate numerical approaches have been given by Glass, Özisik, McRae, and Vick (1986) and Glass and McRae (1990).

In order to introduce nonlinear effects it is necessary to specify the temperature-dependence of the specific heat c, the thermal conductivity k and the relaxation time τ. In order to keep the numerics as simple as possible, we have taken c and τ to be constant and the thermal conductivity to be given by the linear law

$$k = k(\theta) = k_o \left(1 + \beta \frac{\theta - \theta_o}{\theta_o}\right) \ , \tag{3.2}$$

where the constant k_o is the thermal conductivity at the undisturbed state and the nondimensional constant β may be either positive or negative. It is of interest to note that the model used here is identical to that of Glass, Özisik, McRae, and Vick (1986). Furthermore, if we combine (3.2) with the definition (2.3), we find that $2\Gamma = \beta$. Thus, the transformation between their work and ours is relatively straightforward.

4. General Shock Evolution

In each of the examples presented in Sections 5 and 6, we will need to describe the interaction of a shock wave with the thermal waves immediately ahead of and behind the shock. In this section we derive the main interaction formulas. In addition to the formulas listed in Section 2, a key point, which will be used implicitly throughout the following discussion, is that the smooth parts of the disturbance are unaffected by the presence of the shock. Thus, the values of q_1, q_2 or u_1, u_2 will simply be the values carried by the characteristic lines which intersect the shock at that point.

We begin by considering the shock and two characteristics sketched in Figure 4.1. For now we will assume that the disturbance immediately ahead of the shock, i.e., to the right of the shock, is identically zero. The resultant solution will correspond to a shock propagating into an otherwise undisturbed media. We may therefore write the shock slope formula (2.16) as

$$\frac{d\chi_s}{d\xi} = -sgn(\Gamma)\frac{u_s}{2} \tag{4.1}$$

where we have written $u_1 = 0$, $u_2 = u_s$ and u_s can then be regarded as a measure of the shock strength.

The quantity u_s can be related to the boundary data through use of the second, i.e., left-most, characteristic sketched in Figure 4.1. We note that it intersects the $x = 0$ axis at $t = t_o$, or in terms of $\chi - \xi$ coordinates, the point $\xi = 0$, $\chi = \chi_o \equiv t_o/T$. Thus, (2.12) can be written as

$$\begin{aligned} u &= \mathcal{F}(\chi_o) \\ \chi &= \chi_o - sgn(\Gamma)\mathcal{F}(\chi_o)\xi. \end{aligned} \tag{4.2}$$

If we evaluate (4.2) at the shock, we see that the strength of the shock is simply given by the value of $\mathcal{F}$ at the time at which the characteristic intersects the $x = 0$ axis. The shock strength u_s varies because it is struck by different characteristics, each carrying different values of $\mathcal{F}$. The variation of the shock strength with x or ξ is therefore due to the variation of $\mathcal{F}$ from characteristic to characteristic and the rate at which the characteristics catch up to and collide with the shock. The latter effect is due to the distortion of the characteristic lines and the rate at which the shock moves through the characteristic lines which in turn is determined by the shock speed.

The rate at which the characteristics intersect the shock can be computed by noting that there is a unique intersecting characteristic and therefore a unique value of χ_o corresponding to each point on the shock. We denote the relation between this unique χ_o and the value of ξ where the characteristic intersects the shock by $\chi_{os} \equiv \chi_{os}(\xi)$. Thus, if we evaluate (4.2) at the shock, we have

$$u_s = u_s(\xi) = \mathcal{F}\left(\chi_{os}(\xi)\right)$$

$$\chi_s = \chi_{os}(\xi) - sgn(\Gamma)\mathcal{F}\left(\chi_{os}(\xi)\right), \tag{4.3}$$

where $\chi_s = \chi_s(\xi)$ is recognized as the shock trajectory in the $\chi - \xi$ plane. We now differentiate this expression for χ_s with respect to ξ, which yields

$$\frac{d\chi_s}{d\xi} = \frac{d\chi_{os}}{d\xi}\left\{1 - sgn(\Gamma)\mathcal{F}'\xi\right\} - sgn(\Gamma)\mathcal{F}, \tag{4.4}$$

where $\mathcal{F}'(\chi_o) \equiv d\mathcal{F}/d\chi_o$. We may now incorporate the influence of the shock speed and the conditions behind the shock by combining (4.4) with (4.1) to eliminate $d\chi_s/d\xi$. After rearrangement, we find that the equation for $d\chi_{os}/d\xi$ is

$$\frac{d\chi_{os}}{d\xi} = \frac{sgn(\Gamma)}{2} \frac{\mathcal{F}}{1 - sgn(\Gamma)\mathcal{F}'\xi} \ , \tag{4.5}$$

where u_s in (4.1) was replaced by $\mathcal{F}$ through use of the first of (4.3). We note that $\mathcal{F}$ is a known function of χ_{os} once the heat source is specified. Thus, (4.5) is a single ordinary differential equation for $\chi_{os}(\xi)$. Once (4.5) is solved, the shock strength variation $u_s = u_s(\xi)$ and the trajectory $\chi_s = \chi_s(\xi)$ is given by substitution of $\chi_{os}(\xi)$ in (4.3). A simple interpretation of Equation (4.5) is that it gives the rate at which the characteristic lines catch up to the shock.

Equation (4.5) is easily integrated to obtain $\xi = \xi(\chi_{os})$: the result is

$$\xi = \xi_i \left(\frac{\mathcal{F}_i}{\mathcal{F}}\right)^2 + 2\frac{sgn(\Gamma)}{\mathcal{F}^2} \int_{\chi_{oi}}^{\chi_{os}} \mathcal{F}(\lambda) d\lambda, \tag{4.6}$$

where it has been assumed that $\chi_{os} \to \chi_{oi}$ as $\xi \to \xi_i$. Here the constants χ_{oi}, ξ_i can be regarded as the values of χ_{os} and ξ at the beginning of the interaction of interest. The quantity $\mathcal{F}_i \equiv \mathcal{F}(\chi_{oi})$ and λ is simply an integration variable.

We note that the first term in (4.6) typically vanishes when an admissible discontinuity is introduced by the heat source due to the fact that the interaction begins immediately; as a result $\xi_i = 0$.

If no discontinuities are introduced by the heat sources, the shock forms during the course of the evolution. In Part I the values of ξ and χ_o corresponding to formation were written as ξ_F and χ_{oF}, respectively, and were found to be

$$\xi_F = \frac{sgn(\Gamma)}{\mathcal{F}'(\chi_{oF})} \ , \tag{4.7}$$

where χ_{oF} satisfies

$$\mathcal{F}''(\chi_{oF}) = 0 \quad \text{and} \quad sgn(\Gamma)\mathcal{F}'(\chi_{oF}) > 0. \tag{4.8}$$

Again the primes denote derivatives of $\mathcal{F}$ with respect to its argument χ_o. Because the formation point is the initial point for shock evolution, (4.6) may be rewritten as

$$\xi = \frac{sgn(\Gamma)}{\mathcal{F}^2(\chi_{os})}\left[\frac{\mathcal{F}^2(\chi_{oF})}{\mathcal{F}'(\chi_{oF})} + 2\int_{\chi_{oF}}^{\chi_{os}} \mathcal{F}(\lambda)d\lambda\right], \tag{4.9}$$

in this case.

It is of interest to note that an initial condition for (4.5) which is consistent with (4.7) will lead to (4.5) becoming singular. However, inspection of (4.9) reveals that this singularity is integrable. In fact, either (4.5) or (4.9) can be used to verify that

$$\chi_{os} - \chi_{oF} = 0\,(\xi - \xi_F)^{\frac{1}{3}}$$

as $\chi_{os} \to \chi_{oF}$, $\xi \to \xi_F$. It can therefore be shown that the right-hand side of (4.5) has a $(\chi_{os} - \chi_{oF})^{-2} = 0\,(\xi - \xi_F)^{-\frac{2}{3}}$ singularity as $\xi \to \xi_F$.

An important class of interactions is that between shock waves and centered fans. Such fans were discussed in Section 8 of Part I and are the result of the insertion of an inadmissible discontinuity in the initial disturbance. Although one can treat the interaction of a shock with a fan using (4.6) along with a reinitialization which is applied once the fan has had time to spread into a finite width wave, the approach taken here will be to rederive the interaction equation for the special case of a fan.

We begin by recalling that the fan is initiated by a discontinuity. Thus, all the characteristic lines that comprise the fan emanate from a single point. As a result, the parameter χ_o in the description (4.2) no longer has a unique value for each characteristic line and is therefore no longer a useful label for the characteristics. The typical choice for a label is the disturbance value, either u or q, carried by the characteristic. We make this choice and therefore rewrite (4.2) as

$$\chi = \chi_{oCF} - sgn(\Gamma)\xi u, \tag{4.10}$$

where $\mathcal{F}$ has been replaced by u and the fan has been assumed to originate at $\xi = 0$, $\chi = \chi_{oCF}$(= constant).

Now that the description of the fan, i.e., the wave which interacts with shock, has been specified, we may now follow the same steps as used to derive (4.5). When (4.10) is evaluated at the shock, we have

$$\chi_s = \chi_{oCF} - sgn(\Gamma)\xi u_s. \tag{4.11}$$

If we now differentiate (4.11), noting that χ_{oCF} is a numerical constant, and eliminate $d\chi_s/d\xi$ between the resultant equation and (4.1), we find that the equation for u_s is

$$\frac{du_s}{d\xi} = -\frac{u_s}{2\xi}\,, \tag{4.12}$$

which can be immediately integrated to yield

$$u_s = u_i\sqrt{\frac{\xi_i}{\xi}}, \tag{4.13}$$

where we have taken $\xi = \xi_i$ when $u = u_i$. The constants ξ_i, u_i are typically taken to be the initial value of ξ and u at the beginning of the interaction. The shock trajectory is given by substitution of (4.13) in (4.11).

The assumption made at the beginning of this section was that the disturbances in q and θ were always identically zero immediately ahead of the shock. The only place a distinction between conditions before and after the shock was made was in the expression for the shock speed (2.9) or (2.16). However, (4.1) has exactly the same form regardless of whether u_1 or u_2 is used for u_s and we conclude that the main results (4.6), (4.9) and (4.13) are also valid as long as the disturbance in q and θ is identically zero on one side of the shock or the other.

The last case considered here is that where we relax the constraint that the disturbance vanishes either immediately ahead of or behind the shock; this, of course, is the general case. The analysis is essentially the same as that already presented. The main difference is that the general shock slope formula (2.16) must be employed and two parametric formulas similar to (4.2) must be employed. The latter reads

$$u = \mathcal{F}(\chi_{o1}) \text{ on } \chi = \chi_{o1} - sgn(\Gamma)\mathcal{F}(\chi_{o1})\xi$$

$$\tag{4.14}$$

$$u = \mathcal{F}(\chi_{o2}) \text{ on } \chi = \chi_{o2} - sgn(\Gamma)\mathcal{F}(\chi_{o2})\xi,$$

where χ_{o1} and χ_{o2} are the values of χ at which the two characteristic lines intersect the $\xi = 0$, i.e., $x = 0$, axis; we note that the $\mathcal{F}(\lambda) = 0$, when $\lambda < 0$ condition permits us to recover the case where $q_1 = 0$. The subscripts 1 and 2 denote characteristic lines which intersect the shock immediately ahead of and behind the shock. A sketch of typical characteristics and a shock is given in Figure 4.1. When an analysis similar to that presented for the $q_1 = 0$ case is carried out, we find that the shock evolution is governed by the simultaneous equations

$$\frac{d\chi_{os1}}{d\xi} = \frac{sgn(\Gamma)}{2}\frac{\mathcal{F}(\chi_{os1}) - \mathcal{F}(\chi_{os2})}{1 - sgn(\Gamma)\mathcal{F}'(\chi_{os1})\xi},$$

$$\tag{4.15}$$

$$\frac{d\chi_{os2}}{d\xi} = \frac{sgn(\Gamma)}{2} \frac{\mathcal{F}(\chi_{os2}) - \mathcal{F}(\chi_{os1})}{1 - sgn(\Gamma)\mathcal{F}'(\chi_{os2})\xi},$$

where the quantities χ_{os1}, χ_{os2} play the same role as they did in the $u_1 = 0$ and $u_2 = 0$ cases. As in the previous cases, the functions $\mathcal{F}$ and $\mathcal{F}' \equiv d\mathcal{F}/d\chi_o$ are known once the heat source is specified. Thus, (4.15) are solvable either in closed form or through use of numerical integration. The shock trajectory and strength variations are given by evaluating (4.14) at the shock. The trajectory can be obtained by either of the characteristic formulas and can be written

$$\chi_s = \chi_s(\xi) = \chi_{os1} - sgn(\Gamma)\mathcal{F}(\chi_{os1})\xi \tag{4.16a}$$

or

$$\chi_s = \chi_s(\xi) = \chi_{os2} - sgn(\Gamma)\mathcal{F}(\chi_{os2})\xi, \tag{4.16b}$$

which can be computed once (4.15) is solved for $\chi_{os1}(\xi)$ and $\chi_{os2}(\xi)$. The value of u_1 and u_2 are given by

$$u_1 = u_1(\xi) = \mathcal{F}(\chi_{os1}) \quad \text{and} \quad u_2 = u_2(\xi) = \mathcal{F}(\chi_{os2}). \tag{4.17}$$

It is easily verified that the second of (4.15) reduces to (4.5) when $u_1 = \mathcal{F}(\chi_{os1}) = 0$ for all χ_{o1}.

5. Square-Wave Heat Input

The first example to be considered is a square wave heat source of the form

$$\mathcal{F}\left(\frac{t}{T}\right) \equiv \begin{cases} 0 & \text{for} \quad t < 0 \\ 1 & \text{for} \quad 0 < t < T \\ 0 & \text{for} \quad T < t. \end{cases} \tag{5.1}$$

We take the temperature variations of the specific heat, relaxation time, and thermal conductivity to be such that $\Gamma > 0$. As a result the discontinuity introduced by (5.1) at $t = 0$ is admissible and it will therefore propagate as a temperature-raising shock. The switch-off discontinuity at $t = T$ lowers the temperature and is therefore inadmissible. Thus, the discontinuity at the trailing edge of the wave will spread to form a centered fan. The main wave features of a typical evolution are sketched in Figure 5.1. The $x - t$ diagram is given in Figure 5.1(a) and, for reference, the $\chi - \xi$ diagram is given in Figure 5.1(b).

The shock propagates into the undisturbed medium and, in the $\chi - \xi$ plane, its trajectory is a straight line having equation

$$\chi_s = -\frac{1}{2}\xi \tag{5.2}$$

which can be obtained by integration of (2.16) with $u_1 = 0$, $u_2 = 1$ or by substitution of $\xi_i = 0$, $\chi_{oi} = 0$, $\mathcal{F} = 1, sgn(\Gamma) = 1$ in (4.6) to obtain $\chi_{os} = \xi/2$ which is then substituted in (4.3). The first characteristic of the centered fan has the equation

$$\chi = 1 - \xi, \tag{5.3}$$

which is derived by setting $\mathcal{F} = 1$, $\chi_o = 1$ in (4.2). The point (denoted by a subscript c in Figure 5.1) where the centered fan first catches the shock is given by equating the values of χ given in (5.2) and (5.3) to determine χ_s at ξ_c. The resultant values of ξ and χ at which the fan begins to interact with the shock are found to be

$$\xi_c = 2 \quad \text{and} \quad \chi_c = -1. \tag{5.4}$$

The values of x and t at which this occurs are obtained by substitution in (2.14)-(2.15). The result of this substitution is

$$x_c = 2L_s \ln\left(\frac{B_c}{B_c - 1}\right), \tag{5.5}$$

$$t_c = \frac{x_c}{U_o} + \frac{L}{U_o}\chi_c, \tag{5.6}$$

where

$$B_c \equiv \frac{2\epsilon|\Gamma|}{\delta\xi_c}. \tag{5.7}$$

In Section 7 of Part I we found that shock formation was only possible if the relaxation was sufficiently weak compared to the nonlinearity. In like manner we find here that the value of x_c is real only if $B_c > 1$, i.e.,

$$0 < \delta < \frac{2\epsilon|\Gamma|}{\xi_c}. \tag{5.8}$$

If the relaxation parameter is too large and violates (5.8), the temperature-lowering fan sketched in Figure 5.1(a) never catches the shock wave. At large distances from the source the large damping causes both the speed of the shock and the first wave of the fan to approach the speed of the linear theory, i.e., U_o. In the limit of large propagation distances, the spacing between these two waves approaches

$$x_s - x_{fan} \sim L\left(1 - \frac{\epsilon|\Gamma|}{\delta}\right),$$

where x_s is the position of the shock and x_{fan} is the position of the first characteristic of the fan. Clearly, $x_s - x_{fan}$ remains > 0 if (5.8) is violated.

If δ is so large that (5.8) is violated, then the disturbance consists of a leading shock which takes u from 0 to 1, a constant u region which is then followed by a linear decrease of u with ξ through the centered fan; this trapezoidal disturbance persists for all ξ and its counterpart in the q, x, t variables persists for all time. In terms of the latter variables, the $0 < B_c < 1$ solution can be shown to be

$$\frac{q}{q_m} = \begin{cases} 0 & \text{for} \quad 0 < \frac{t}{T} < \frac{x}{L} - \hat{\xi} \\ e^{-\frac{x}{2L_s}} & \text{for} \quad \frac{t}{T} > \frac{x}{L} - \hat{\xi} \end{cases} \tag{5.9}$$

if $0 < t < T$ and is given by

$$\frac{q}{q_m} = \begin{cases} 0 & \text{for} \quad 1 < \frac{t}{T} < \frac{x}{L} - \hat{\xi} \\ e^{-\frac{x}{2L_s}} & \text{for} \quad \frac{x}{L} - \hat{\xi} < \frac{t}{T} < \frac{x}{L} + 1 - 2\hat{\xi} \\ \frac{L - U_o t + x}{2L\hat{\xi}} e^{-\frac{x}{2L_s}} & \text{for} \quad \frac{x}{L} + 1 - 2\hat{\xi} < \frac{t}{T} < 1 + \frac{x}{L} \\ 0 & \text{for} \quad \frac{t}{T} > 1 + \frac{x}{L}, \end{cases} \tag{5.10}$$

when $t > T$. Here

$$\hat{\xi} \equiv \frac{\xi}{\xi_c} = B_c \left(1 - e^{-\frac{x}{2L_s}}\right). \tag{5.11}$$

The solution (5.9) is that which holds before the whole thermal wave of duration T separates from the heater and (5.10) is the solution holding after the heater switches off. In (5.9) and (5.10), the limit $x - \hat{\xi}L$ is recognized as the $x - t$ counterpart of (5.2) and the limit $x + L - 2\hat{\xi}L$ is the $x - t$ version of (5.3). The $x - t$ version of the centered fan described in Section 8 of Part I occupies the third region of (5.10).

If $B_c > 1$, i.e., if the relaxation is sufficiently weak compared to the nonlinearity, the fan begins to interact with the shock at values of x_c and t_c given by (5.5)-(5.6). After this takes place, the disturbance is simply a temperature-raising shock which is followed by the centered fan. The interaction between the fan and shock weakens the shock and the strength variation is given by (4.13) with $\xi_i = \xi_c$ and $u_i = 1$. As pointed out in Section 4, the shock trajectory is determined by combining (4.13) with (4.11). In terms of $x - t$ variables, the solution for the $B_c > 1$ case is therefore given by

$$\frac{q}{q_m} = \begin{cases} 0 & \text{for} \quad 1 < \frac{t}{T} < \frac{x}{L} + 1 - 2\sqrt{\hat{\xi}} \\ \frac{L - U_o t + x}{2L\hat{\xi}} e^{-\frac{x}{2L_s}} & \text{for} \quad 1 + \frac{x}{L} - 2\sqrt{\hat{\xi}} < \frac{t}{T} < 1 + \frac{x}{L} \\ 0 & \text{for} \quad \frac{t}{T} > 1 + \frac{x}{L}, \end{cases} \tag{5.12}$$

if $t > t_c$, where $\hat{\xi}$ is again given by (5.11). The solution for $B_c > 1$, $t < t_c$ is just that given by (5.9)-(5.10).

It should be noted that the form chosen in (5.9)-(5.12) is particularly useful if t is fixed and the q vs x distribution is desired. If we desire q vs t at fixed x a slight modification of this format may be desirable.

To illustrate the evolution predicted by (5.9)-(5.12), we have plotted q/q_m vs x/L at various times in Figure 5.2. The solution is compared to the numerical solution of the exact Maxwell-Cattaneo equations as described in Section 3. The parameters used were $\epsilon|\Gamma| = 0.1$, $\delta = 0.01$. As a result, $B_c = 10$ and $x_c \approx 21L$, $t_c \approx 20T$. Inspection of Figure 5.2 reveals that the pure numerical solution agrees well (with the exception of the usual numerical oscillations at shocks) with the weak shock theory developed here.

In Figure 5.3, we have reconsidered the same case but have plotted the temporal variation of the heat flux at fixed x locations. This choice illustrates the time signatures one would expect to observe in typical experimental configurations where the measurements are carried out at fixed positions in the test specimen.

In Figure 5.4, we have plotted the variation of the shock strength with distance from the source. In terms of the u, χ, ξ variables, $u_s = 1$ before the fan interacts with the shock and, as pointed out earlier, is given by (4.13) after the interaction takes place. In terms of the q, x, t variables, we have

$$\frac{q_s}{q_m} = \begin{cases} e^{-\frac{x}{2L_s}} & \text{for} \quad 0 < x < x_c \\ \frac{e^{-\frac{x}{2L_s}}}{\sqrt{\hat{\xi}}} & \text{for} \quad x > x_c, \end{cases} \tag{5.14}$$

where $\hat{\xi}$ is given by (5.11). The $\hat{\xi}^{-\frac{1}{2}}$ factor increases the decay of the shock. Thus, nonlinear effects lead to a stronger decay than that predicted by the linear theory. In fact, we can shown that

$$\hat{\xi} \to \frac{\epsilon|\Gamma|}{\xi_c}\frac{x}{L} = \frac{\epsilon|\Gamma|}{2}\frac{x}{L} \tag{5.15}$$

as $\delta \to 0$ with fixed x. The $x > x_c$ behavior in (5.14) can then be written

$$\frac{q_s}{q_m} \to \left(\frac{2L}{\epsilon|\Gamma|x}\right)^{\frac{1}{2}},$$

which is the classical shock decay law for the $\delta = 0$ ($\tau_o \to \infty$) form of the Varley-Rogers equation (2.1). We conclude that the nonlinearity would lead to wave decay even if the relaxation is negligible. When δ satisfies (5.8), the final decay is a combination of the two effects.

Finally, we plot the time of arrival of the disturbance as a function of specimen length H in Figure 5.5. Here we take the arrival time for the disturbance to be the time at which the shock arrives at the end of the specimen, i.e., at $x = H$. It is easily verified that the shock arrival times t_{arr} can be written

$$\frac{U_o t_{arr} - H}{L} = \begin{cases} -B_c\left(1 - e^{-\frac{H}{2L_s}}\right) & \text{for} \quad 0 < H < x_c \\ 1 - \xi_c B_c^{\frac{1}{2}}\left(1 - e^{-\frac{H}{2L_s}}\right)^{\frac{1}{2}} & \text{for} \quad H > x_c, \end{cases} \tag{5.16}$$

where ξ_c and x_c are given by (5.4)-(5.5). Inspection of Figure 5.5 reveals that the shock always arrives before the time predicted by the linear theory. This should be expected when one recalls the discussion in Section 8 of Part I where it was pointed out that the speed of the temperature-raising shock is the average of the thermal wave speeds immediately ahead of and behind the shock. Because there is no disturbance immediately ahead of the shock, the thermal wave speed there is exactly equal to the linear wave speed U_o and the shock speed is therefore always greater than U_o.

We note that the case where (5.8) is violated is contained in (5.14) and (5.16). In such a case we can simply regard x_c as being infinite. As a result, only the first solution in (5.14) and (5.16) should be used.

Because the arrival time formulas given in (5.16) involve the intrinsic material nonlinearity $|\Gamma|$ in a relatively simple way, we offer the speculation that measurements of the arrival times might be a useful way to evaluate the accuracy of the constitutive theory. As pointed out by Tarkenton and Cramer (1994) and in Part I, many competing constitutive theories are indistinguishable in the linear limit, thus such arrival time measurements may in fact be a useful way to eliminate incorrect constitutive assumptions. Even in the context of the Maxwell-Cattaneo theory, the assumed or estimated variations of τ, c and k with temperature can be checked or even refined through use of arrival time data.

Throughout this section we have taken $\Gamma > 0$ which has strongly influenced the nature of the evolution of the disturbance. However, the analysis for the $\Gamma < 0$ case is essentially the same as that presented so far. The main difference in the evolution is that the temperature-raising discontinuity generated at $t = 0$ is inadmissible and spreads to form a centered fan. The temperature-lowering discontinuity generated at $t = T$ is admissible and propagates as a shock. Before the fan begins to interact with the shock (provided it does so) the disturbance is headed by the linear increase in u through the fan from $u = 0$ to $u = 1$. A $u = 1$ region follows the fan; this region is terminated by the temperature-lowering shock which is initiated at $t = T$. After the shock catches the fan the disturbance is simply a linear increase in u terminated by the shock. This disturbance is simply an inverted (in space) version of the $\Gamma > 0$ wave. The condition (5.8) is still required in order that the fan interacts with the shock.

In the interests of completeness we will simply record the solution for the $\Gamma < 0$ case. If $0 < t < T$ we have

$$\frac{q}{q_m} = \begin{cases} 0 & \text{for} \quad \frac{x}{L} > \frac{t}{T} > 0 \\ \frac{U_o t - x}{2L\hat{\xi}} e^{-\frac{x}{2L_s}} & \text{for} \quad \frac{x}{L} + 2\hat{\xi} > \frac{t}{T} > \frac{x}{L} \\ e^{-\frac{x}{2L_s}} & \text{for} \quad 1 > \frac{t}{T} > \frac{x}{L} + 2\hat{\xi}, \end{cases} \tag{5.17}$$

where $\hat{\xi}$ is again given by (5.11). The solution for $T < t < t_c^-$ is

$$\frac{q}{q_m} = \begin{cases} 0 & \text{for} \quad \frac{x}{L} > \frac{t}{T} > 0 \\ \frac{U_o t - x}{2L\hat{\xi}} e^{-\frac{x}{2L_s}} & \text{for} \quad \frac{x}{L} + 2\hat{\xi} > \frac{t}{T} > \frac{x}{L} \\ e^{-\frac{x}{2L_s}} & \text{for} \quad \frac{x}{L} + 1 + \hat{\xi} > \frac{t}{T} > \frac{x}{L} + 2\hat{\xi} \\ 0 & \text{for} \quad \frac{t}{T} > \frac{x}{L} + 1 + \hat{\xi}, \end{cases} \tag{5.18}$$

and finally, for $t > t_c^-$,

$$\frac{q}{q_m} = \begin{cases} 0 & \text{for} \quad \frac{x}{L} > \frac{t}{T} > 0 \\ \frac{U_o t - x}{2L\hat{\xi}} e^{-\frac{x}{2L_s}} & \text{for} \quad \frac{x}{L} + 2\sqrt{\hat{\xi}} > \frac{t}{T} > \frac{x}{L} \\ 0 & \text{for} \quad 1 > \frac{t}{T} > \frac{x}{L} + 2\sqrt{\hat{\xi}}, \end{cases} \tag{5.19}$$

where x_c is again given by (5.5) and

$$t_c^- \equiv 2T + \frac{x_c}{U_o} \tag{5.20}$$

is the time at which the temperature-raising fan first intersects the temperature-lowering shock. Again the specific form used for the presentation of (5.17)-(5.20) is best suited for plotting q vs x at fixed t.

The shock strength variation is essentially the same as that for the $\Gamma > 0$ case. Because the shock is formed at the back of the wave, the front of the wave travels at the linear wave speed U_o. Therefore the time required for the wave to travel a distance H will always be H/U_o.

6. Sine-Wave Heat Input

We now consider a heat source of the form

$$\mathcal{F}\left(\frac{t}{T}\right) \equiv \begin{cases} sin\frac{2\pi t}{T} & \text{for} \quad 0 < t < T \\ 0 & \text{otherwise,} \end{cases} \tag{6.1}$$

which is recognized as a finite length sine pulse. Because (6.1) is smooth, the shock waves which occur are those which form due to the nonlinear steepening. In the range $0 < t < T$, the first and second derivatives of $\mathcal{F}(\chi_o)$ are $2\pi cos(2\pi\chi_o)$ and $-4\pi^2 \sin(2\pi\chi_o)$, respectively. The values of $\chi_o(= \chi_{oF})$ satisfying (4.8) are

$$\begin{aligned} \chi_{oF} &= 0 \text{ and } 1, \quad \text{if} \quad \Gamma > 0 \\ \chi_{oF} &= \tfrac{1}{2} \qquad\quad \text{if} \quad \Gamma < 0. \end{aligned} \tag{6.2}$$

Thus, the shock forms near the front and rear of the sine wave if $\Gamma > 0$ and near the middle node if $\Gamma < 0$. In either case, it can be shown that (4.7) may be written

$$\xi_F = \frac{1}{2\pi}. \tag{6.3}$$

In Section 7 of Part I, we derived the criterion for shock formation. When (6.3) is employed we find that shocks form only if

$$B_F \equiv \frac{4\pi\epsilon|\Gamma|}{\delta} > 1 \tag{6.4}$$

for either sign of Γ. The corresponding position at which the shock forms is given by

$$x_F = 2L_s \ln\left(\frac{B_F}{B_F - 1}\right). \tag{6.5}$$

The time at which formation occurs can be derived from the equation of the characteristic line in (2.12). If we take this characteristic line to be that which goes through the point $\xi = 0$, $\chi = \chi_{oF}$, i.e., it is the characteristic line at which shock formation occurs, we have

$$\chi = \chi_{oF} - sgn(\Gamma)\xi\mathcal{F}(\chi_{oF}). \tag{6.6}$$

If we now evaluate (6.6) at the formation point $\xi = \xi_{_F}$, $\chi = \chi_{_F}$, and use the definition (2.15), we have

$$t_{_F} = \frac{x_{_F}}{U_o} + T\chi_{_{oF}} - sgn(\Gamma)T\xi_{_F}\mathcal{F}(\chi_{_{oF}}). \tag{6.7}$$

For both $\Gamma < 0$ and $\Gamma > 0$, $\mathcal{F}(\chi_{_{oF}}) = 0$. As a result, (6.7) becomes $t_{_F}{=}x_{_F}/U_o{+}T\chi_{_{oF}}$. Thus, if $\Gamma > 0$

$$t_{_F} = \frac{x_{_F}}{U_o} \quad \text{and} \quad \frac{x_{_F}}{U_o} + T \tag{6.8}$$

for the front and rear shocks, respectively. If $\Gamma < 0$ then

$$t_{_F} = \frac{x_{_F}}{U_o} + \frac{1}{2}. \tag{6.9}$$

As a numerical example, we consider the case where $\delta = 0.1, \epsilon|\Gamma| = 0.05$, which yields $B_{_F} = 2\pi > 1$. Substitution of the values for δ and $B_{_F}$ in (6.5) yields $x_{_F} = 3.47L$ for each case. If $\Gamma > 0$, then (6.8) yields $t_{_F} = 3.47T$ and $4.47T$ and if $\Gamma < 0$, (6.9) yields $t_{_F} = 3.97T$.

The solution for $0 < x < x_F$ can now be written in the parametric form

$$\begin{aligned} \frac{q}{q_m} &= \mathcal{F}(\chi_o)e^{-\frac{x}{2L_s}} \\ \frac{t}{T} &= \frac{x}{L} + \chi_o - sgn(\Gamma)\xi\mathcal{F}(\chi_o), \end{aligned} \tag{6.10}$$

where the constants in (2.12) were evaluated by setting $u = \mathcal{F}(\chi_o)$, $\chi = \chi_o$ at $\xi = 0$ and (2.13)-(2.15) were employed. The solution (6.10) also holds for all $x > 0$ in the case where no shock forms, i.e., $B_F < 1$. Throughout this section we will present our results as time histories at a fixed x and therefore use the range of x to specify the solutions.

After the shocks form, the $\Gamma < 0$ case and the $\Gamma > 0$ case must be treated differently. In the $\Gamma > 0$ case, each shock has either u_1 or u_2 equal to 0 and (4.9) may therefore be employed. In the case where $\Gamma < 0$, the shock forms in the middle of the sine wave and the general solution (4.15) must be used. In the following discussion, we develop each of these solutions separately.

We first consider the case where $\Gamma > 0$. The wave structure in the $x - t$ plane has been sketched in Figure 6.1. If we use (6.1)-(6.2) it is easily demonstrated that $\mathcal{F}(\chi_{oF}) = 0$ and that (4.9) can be written

$$\xi = \frac{2}{\mathcal{F}^2(\chi_{os})} \int_{\chi_{oF}}^{\chi_{os}} \mathcal{F}(\lambda) d\lambda. \tag{6.11}$$

It can also be shown that the only part of (6.1) which is useful is that between $t = 0$ and $t = T$. Thus, (6.11) can be integrated to yield

$$\xi = \frac{1}{\pi} \frac{1 - \cos 2\pi\chi_{os}}{\sin^2 2\pi\chi_{os}} = \frac{1}{\pi} \frac{1}{1 + \cos 2\pi\chi_{os}}. \tag{6.12}$$

If we invert (6.12) for $\chi_{os} = \chi_{os}(\xi)$, we find that the two roots are given by

$$\chi_{os} = \frac{1}{2\pi} \cos^{-1}\left(\frac{2\xi_F}{\xi} - 1\right), \tag{6.13}$$

where (6.3) has been used. Because the argument of the $\cos^{-1}$ function varies between -1 and 1 for all $\xi > \xi_F$, the roots (6.13) are always real.

If we denote the two values of χ_{os} obtained from (6.13) at a fixed ξ by $\chi_{os}^{(1)}$ and $\chi_{os}^{(2)}$, it can be shown that these can be chosen to satisfy

$$\begin{gathered} 0 < \chi_{os}^{(1)} < \frac{1}{2}, \\ \\ \frac{1}{2} < \chi_{os}^{(2)} = 1 - \chi_{os}^{(1)} < 1. \end{gathered} \tag{6.14}$$

It can also be shown that the root $\chi_{os}^{(1)}(\xi)$ will correspond to the lead shock and the root $\chi_{os}^{(2)}(\xi)$ will correspond to the trailing shock.

It turns out that the actual range taken on by $\chi_{os}^{(1)}$ and $\chi_{os}^{(2)}$ is smaller than that indicated by (6.14). The correct range can be determined by inspection of the transform (2.14). We note that ξ varies between 0 and

$$\xi_m \equiv \frac{2\epsilon|\Gamma|}{\delta} = B_F \xi_F \tag{6.15}$$

as x varies between 0 and ∞. Here (6.3) and (6.4) have been employed. Thus,

$$-1 < \frac{2}{B_F} - 1 < \frac{2\xi_F}{\xi} - 1 < 1, \tag{6.16}$$

in the range $x_F < x < \infty$. As a result, (6.14) can be rewritten

$$\begin{gathered} 0 < \chi_{os}^{(1)} < \chi_{os}^{(m)} < \frac{1}{2} \\ \text{and} \\ \frac{1}{2} < 1 - \chi_{os}^{(m)} < \chi_{os}^{(2)} = 1 - \chi_{os}^{(1)} < 1, \end{gathered} \tag{6.17}$$

where the constant $\chi_{os}^{(m)}$ satisfies

$$\chi_{os}^{(m)} = \frac{1}{2\pi}\cos^{-1}\left(\frac{2}{B_F} - 1\right) \quad \text{and} \quad 0 < \chi_{os}^{(m)} < \frac{1}{2}. \tag{6.18}$$

The interpretation of the existence of the limiting value of χ_{os} in (6.18) is that not all the characteristics originating at the $x = 0$ axis and in the range $0 < t < T/2$ catch up to the lead shock. In like manner, not all the characteristics originating at $x = 0$, $T/2 < t < T$ intersect the trailing shock. When the damping is weak relative to the nonlinearity, B_F is large and $\chi_{os}^{(m)} \to 1/2$ from below which implies that most of the characteristics in the range $0 < \chi_o < 1/2$ intersect the head shock and that most of the characteristics in the range $1/2 < \chi_o < 1$ intersect the trailing shock. This is consistent with the $\delta = 0$ theory in which *all* of the characteristics in the range $0 < \chi_o < 1$ intersect one shock or the other. When δ is close to the limiting value $4\pi\epsilon|\Gamma|$, $B_F \approx 1$, $\chi_{os}^{(m)}$ approaches zero and only a very small range of characteristics intersect either shock. The physical reason is essentially the same as that which prevents shocks from forming when $B_F < 1$. In this case, the damping causes the slopes of all of the characteristics and the shock to approach the zero-amplitude, i.e. linear, slope. Thus, at large propagation distances, the slopes of the characteristics originating in the vicinity of $x = 0$, $t = T/2$ become nearly parallel to the shock and therefore never catch it.

We note that similar limitations on the range of characteristics which interact with the shock can be found for most heat inputs. In fact, such a limitation exists for the centered fan - shock interactions discussed in Section 5. In that case it was not necessary to deal with the limitation explicitly.

The trajectories of the shocks are given by (4.3). If we write these in terms of the x, t coordinates, we find that the trajectories $t_s^{(1)}(x), t^{(2)}(x)$ of the leading and trailing shocks are given by

$$t_s^{(1)} = \frac{x}{U_o} + T\left[\chi_{os}^{(1)} - \frac{\bar{\xi}}{2\pi}\mathcal{F}\left(\chi_{os}^{(1)}\right)\right]$$
$$t_s^{(2)} = \frac{x}{U_o} + T\left[\chi_{os}^{(2)} - \frac{\bar{\xi}}{2\pi}\mathcal{F}\left(\chi_{os}^{(2)}\right)\right], \tag{6.19}$$

where the function $\mathcal{F}$ is given by (6.1) and $\chi_{os}^{(1)}$, $\chi_{os}^{(2)}$ are computed from (6.13) and (6.17) once x, and therefore ξ, are chosen. The quantity

$$\bar{\xi} \equiv \frac{\xi}{\xi_F} = B_F \left(1 - e^{-\frac{x}{2L_s}}\right). \tag{6.20}$$

Because of the limits on $\chi_{os}^{(1)}$, $\chi_{os}^{(2)}$, the relevant part of the function $\mathcal{F}$ in will always turn out to be the nonzero portion of the sine-pulse.

The solution for $\Gamma > 0$, $B_F > 1$ and $x > x_F$ may now be constructed. As pointed out earlier we will fix x and compute the q vs t signatures. The solution may be summarized as follows:

$$q = 0 \qquad \text{when} \qquad 0 < t < t_s^{(1)} \qquad \text{or} \qquad t > t_s^{(2)}. \tag{6.21}$$

When $t_s^{(1)} < t < t_s^{(2)}$ we construct the solution by substituting various values of χ_o from the range $\chi_{os}^{(1)} < \chi_o < \chi_{os}^{(2)}$ in

$$\begin{aligned} \frac{q}{q_m} &= \mathcal{F}(\chi_o)\, e^{-\frac{x}{2L_s}} \\ \frac{t}{T} &= \frac{x}{L} + \chi_o - \frac{\bar{\xi}}{2\pi}\mathcal{F}(\chi_o). \end{aligned} \tag{6.22}$$

A sample calculation employing both (6.21)-(6.22) and the $0 < x < x_F$ solution, i.e., (6.10), is plotted in Figure 6.2. The parameters were taken to be $\epsilon\Gamma = 1/20$ and $\delta = \pi/20$. As a result, $B_F = 4$ and $x_F \approx 3.66L$. The last tw histories at $x = 4.25L$ and $x = 5.75L$ therefore contain shocks at the front and rear. Because $\chi_{os}^{(1)} \approx 0.11$ and 0.19 for these two cases, the local maximum and local minimum of the sine curve has not yet collided with and been absorbed by the shock. Hence these extrema remain visible in the plots. The extrema collide with the shocks when $\chi_{os}^{(1)} = 1/4$ which corresponds to an $x \approx 8.8L$ in this example. After this time the smooth temperature increase vanishes and the wave is headed by a temperature-raising shock followed by a smooth temperature decrease terminated by the trailing shock. We have also compared the weak shock results to the numerical solutions of the full Maxwell-Cattaneo equations. As in the case of the square wave we find reasonable agreement except for the numerical oscillations generated as the shocks begin to form.

In Figure 6.3, we have plotted the strength of the first shock as measured at a fixed x location for various values of B_F. The formula employed is simply

$$\frac{q_s}{q_m} = \mathcal{F}\left(\chi_{os}^{(1)}\right) e^{-\frac{x}{2L_s}}$$

for $x > x_F$, with $\chi_{os}^{(1)}$ given by (6.13)-(6.14). At formation, the shock strength is zero whereupon it grows to some maximum value and then decays due to both relaxation and the interaction with the smooth part of the temperature distribution.

The arrival times of thermal waves are plotted in Figure 6.4 as a function of distance H from the source, i.e., $x = 0$. As in the case of the square waves we take the arrival time to be the time at which the first disturbance arrives at H. In the present case this may be either a shock or the smooth front. The vertical coordinate is the time shifted with the arrival time as predicted by the linear theory, i.e., H/U_o. When H is relatively small, the shock has not formed and the arrival time is just that of the linear theory. Because the speed of the shock is always larger than the linear wave speed U_o, the arrival times are shorter once $H > x_F$.

We now discuss the case where $\Gamma < 0$. The solution for $x < x_F$, as well as the case $0 < B_F < 1$ and $x > 0$ is given by (6.10). As discussed in Part I, the steepening is backwards when $\Gamma < 0$ which results in the formation of a single temperature-lowering shock in the middle of the sine pulse. Mathematically, this formation scenario is expressed by the second of (6.2). Because the values of u and q on each side of the formed shock are nonzero, the shock evolution is necessarily given by (4.15). In general, (4.15) must be solved numerically subject to the initial condition

$$\chi_{os1} = \chi_{os2} = \chi_{oF} = \frac{1}{2} \quad \text{at} \quad \xi = \xi_F = \frac{1}{2\pi}. \tag{6.23}$$

However, the fact that the function $\mathcal{F}$ is anti-symmetric about the point $t = T/2$ can be used to demonstrate that a partial solution of (4.15) and (6.23) is

$$\chi_{os1} + \chi_{os2} = 1. \tag{6.24}$$

When we substitute (6.24) in the shock trajectory formula (4.16) and again use the symmetry properties of (6.1), we find that

$$\chi_s = \frac{1}{2} \tag{6.25a}$$

for all ξ. That is, the shock remains at a fixed position in $\xi - \chi$ coordinates. In $x - t$ coordinates (6.25a) becomes

$$t_s = \frac{x}{U_o} + \frac{T}{2}. \tag{6.25b}$$

which implies that the temperature lowering shock travels with the linear wave speed U_o. If we then substitute (6.25a) in (4.16a), we find that χ_{os1} satisfies

$$\xi = \frac{\frac{1}{2} - \chi_{os1}}{\mathcal{F}(\chi_{os1})}. \tag{6.26}$$

As in the $\Gamma > 0$ case, the range of χ_{os1} is limited due to the fact $0 < \xi < \xi_m$, where ξ_m is again given by (6.15). Thus,

$$0 < \bar{\chi}^{(m)}_{os1} < \chi_{os1} < \frac{1}{2}, \tag{6.27}$$

where the limit value $\bar{\chi}_{os1}^{(m)}$ satisfies (6.26), evaluated at $\xi = \xi_m$, i.e.,

$$\frac{B_F}{2\pi} = \frac{\frac{1}{2} - \bar{\chi}_{os1}^{(m)}}{\mathcal{F}\left(\bar{\chi}_{os1}^{(m)}\right)}. \tag{6.28}$$

The corresponding limit of $\chi_{os2}(\xi)$ can be obtained by combining (6.27)-(6.28) with (6.24). As in the $\Gamma > 0$ case, the interpretation of the limiting χ_{os1} is that only a limited range of characteristics intersect and therefore interact with the shock. In the present case ($\Gamma < 0$) the shock forms in the middle of the pulse and therefore begins by interacting with the characteristics which originate at $t \approx T/2$. If B_F is only slightly greater than one, only the characteristics which originate in the immediate vicinity of $t = T/2$ interact, whereas most of the characteristics interact with the shock if B_F is large. For example, $\bar{\chi}_{os1}^{(m)} \approx 0.1$ when $B_F \approx 4.276$ and $\bar{\chi}_{os1}^{(m)} \approx 0.4$ when $B_F \approx 1.07$.

The solution for the $\Gamma < 0$, $B_F > 1$, $x > x_F$ case may now be written as

$$\frac{q}{q_m} = \mathcal{F}(\chi_o) e^{-\frac{x}{2L_s}}$$

$$\frac{t}{T} = \frac{x}{L} + \chi_o + \frac{\bar{\xi}}{2\pi}\mathcal{F}(\chi_o), \tag{6.29}$$

where $\mathcal{F}$ is given by (6.1) and $\bar{\xi} = \bar{\xi}(x)$ is given by (6.20) and we choose various values of χ_o in the ranges

$$-\infty < \chi_o < \chi_{os1}(\xi) \quad \text{and} \quad \chi_{os2}(\xi) < \chi_o < \infty. \tag{6.30}$$

For a fixed $x > x_F$, i.e., $\xi > \xi_F$, χ_{os1} can be determined from (6.26) by numerical inversion and χ_{os2} is then given by (6.24).

Time histories for a $\Gamma < 0$ case with parameters $\epsilon|\Gamma|$ and δ identical to those of Figure 6.2 are plotted in Figure 6.5. The numerical solutions to the full Maxwell-Cattaneo equations are also included. As in previous examples, the weak shock theory agrees well with the solutions to the exact equations.

The value of q immediately before and after the shock can be obtained by converting (4.17) to q, x, t coordinates. We have plotted the variation of q_1 and q_2 as a function of x in Figure 6.6. One can also consider the arrival times for the $\Gamma < 0$ case. As in the $\Gamma < 0$, square wave case, the front of the wave travels at the linear wave speed U_o and the arrival time at a point $x = H$ from the source is simply H/U_o.

7. Summary

The main goal of the present investigation was to develop explicit solutions for finite width thermal pulses. The basis for these solutions is the weak shock theory developed in Part I and summarized in Section 2 of the present study. The primary new issue which arises when nonlinear waves are considered is the interaction of shock waves with the smooth parts of the temperature distribution. The general description of this interaction was presented in Section 4. In the most general case, the shock evolution is governed by the system (4.15). In general, these equations must be integrated numerically. When the disturbance is identically zero on one side of the shock on the other, (4.15) can be simplified and integrated analytically to yield the χ_{os} vs ξ relation given either by (4.6) or (4.9). The special case of the interaction between a shock and a centered fan is governed by (4.13).

In order to render our discussion concrete, our results were presented for a heat source located at $x = 0$. However, the techniques described here require only minor modifications if solutions for cases where the wave is generated by an initial temperature or heat flux distribution; one only needs to insure that the initial distributions are consistent with the right-running wave condition (2.4). Solutions for an imposed temperature source at $x = 0$ require no modification due to the assumption (2.4).

Examples of the application of the general interaction formulas are provided in Sections 5 and 6. The evolution of pulses initially containing inadmissible discontinuities and those involving the formation of shock waves from smooth profiles were described. When the decay due to relaxation is sufficiently weak compared to the nonlinear steepening, it was shown that nonlinear effects give rise to a stronger decay than that predicted by the linear theory. This point was noted explicitly in our discussions of the evolution of square wave heat inputs in Section 5 and is implicit in the results of Section 6 . In addition to this enhancement of the decay, the interaction between the shock and the rest of the wave typically results in a temperature distribution which differs qualitatively from that of the linear theory.

An interesting phenomenon not found in the undamped ($\delta = 0$) theory or the close analog of ordinary nonlinear acoustics is the inevitable freezing of the profile at large times. Although it can be shown that such freezing occurs even in the square wave problem of Section 5, the explicit discussion is found in Section 6 where the limiting characteristic parameter (6.18) was introduced. The physical reason for the freezing of the profile is that the relaxation damping causes all the wave speeds to approach those of the linear theory at large times or distances. As a result, every portion of the pulse ultimately propagates at the same speed and the nonlinear distortion and interactions are suppressed. Because of the fundamental nature of the competing physical effects, such freezing should be expected for virtually all cases having $\delta > 0$.

Here we observe is that the freezing of the profile is equivalent to stating that the shock only interacts with a portion of the smooth part of the wave. Thus, it may occur that changes to the details of the heat input may never be "felt" by the shock. This fact must be taken into account whenever efforts are made to modify the wave evolution through modifications of the boundary or initial data.

As pointed out in Part I, the solutions were seen to depend on two similarity parameters. The first is the sign of the intrinsic nonlinearity parameter Γ and the second typically involves the combination $\epsilon|\Gamma|/\delta$; specific examples of the latter are given by the similarity parameters (5.7) and (6.4). One way to view this self-similarity is as an expression of the competition between nonlinear steepening and the decay caused by relaxation. Because of the intrinsic importance of these two physical effects, we believe analogous similarity parameters will arise even when different geometries are considered.

Finally, we note that the arrival time formulas developed here may be of use in experiments designed to verify the constitutive theory or the specific temperature dependencies of τ, c, or k. In particular, the square-wave heat input is likely to be one of the easiest to generate in practice. Comparisons of the dependence of the arrival time at fixed distance on the initial amplitude would then reveal any inconsistencies (should they exist) in the exact model.

References

Cramer, M. S. 1994, "Nonlinear thermal waves: Part I- A weak shock theory," submitted for publication to the International Journal of Heat and Mass Transfer.

Glass, D. E. Özisik, M. N., McRae, D. S. and Vick, B. 1986, "Hyperbolic heat conduction with temperature-dependent thermal conductivity," J. Appl. Phys., Vol. 59, No. 6, pp. 1861-1865.

Glass, D. E. and McRae, D. S. 1990, "Variable specific heat and thermal relaxation parameter in hyperbolic heat conduction," J. Thermophysics, Vol. 4, No. 2, pp. 252-255.

Lowekamp, B. B., Watson, L. T., and Cramer, M. S. 1994, "The cellular automata paradigm for the parallel solution of heat transfer problems," Department of Computer Science Technical Report TR 94-15, Virginia Polytechnic Institute and State

University, Blacksburg, Virginia.

Tarkenton, G. M. and Cramer, M. S. 1994, "Nonlinear second sound in solids," Phys. Rev. B, Vol. 49, No. 17, pp. 11794-11798.

Figure Captions

Figure 4.1: Sketch of the $x - t$ diagram for the construction of the shock strength evolution equations.

Figure 5.1: Sketch of (a) the $x - t$ diagram, and (b) the corresponding $\xi - \chi$ diagram for a square-wave heat input. The point marked c denotes the point at which the centered fan generated at $x = 0$, $t = T$ catches up to and begins interacting with the shock.

Figure 5.2: Plot of evolution of a square-wave heat input at various scaled times. Solid lines denote the weak-shock solutions developed here and the dots denote numerical solutions to the exact Maxwell-Cattaneo equations (3.1). The parameters chosen were $\epsilon|\Gamma| = 0.1$ and $\delta = 0.01$.

Figure 5.3: Plot of the time signatures for a square-wave heat input computed at various scaled x locations. Solid lines denote the weak-shock solutions and the dots denote numerical solutions to (3.1). The physical parameters are identical to those of Figure 5.2.

Figure 5.4: Variation of the shock strength as a function of scaled propagation distance for the square-wave heat input. The solid line denotes $B_c = 2$, _______ denotes $B_c = 4$, _______ denotes $B_c = 6$, _______ $B_c = 8$, and _______ denotes $B_c = 10$.

Figure 5.5: Variation of scaled arrival times (t_{arr}) at $x = H$ for the square-wave heat input. Each line type corresponds to the same value of B_c as indicated in Figure 5.4.

Figure 6.1: Sketch of $x - t$ diagram for the finite length sine pulse. Heavy lines denote shock waves and the lighter lines denote characteristic lines.

Figure 6.2: Computed time signatures at various x locations for the finite length sine pulse having $\Gamma > 0$. The solid lines denote the weak-shock solutions and the dots denote numerically generated solutions to (3.1). The values of $\epsilon|\Gamma|$ and δ were $1/20$ and $\pi/20$, respectively.

Figure 6.3: Variation of the lead shock strength as a function of scaled propagation distance. The line ________ denotes $B_F = 2$, ________ denotes $B_F = 3$, ________ denotes $B_F = 4$, ________ denotes $B_F = 5$.

Figure 6.4: Variation of scaled arrival times (t_{arr}) at $x = H$. Each line type corresponds to the same value of B_F as indicated in Figure 6.3.

Figure 6.5: Computed time signatures at various locations for the finite length sine pulse having $\Gamma < 0$. The solid lines denote the weak-shock solutions and the dots denote numerically generated solutions to (3.1). The values of $\epsilon|\Gamma|$ and δ are identical to those of Figure 6.2.

Figure 6.6: Variation of the values of q immediately ahead of and behind the temperature-lowering shock as a function of scaled proportion distance for the finite length sine wave having $\Gamma < 0$. Each line type corresponds to the same value of B_F as indicated in Figure 6.3.

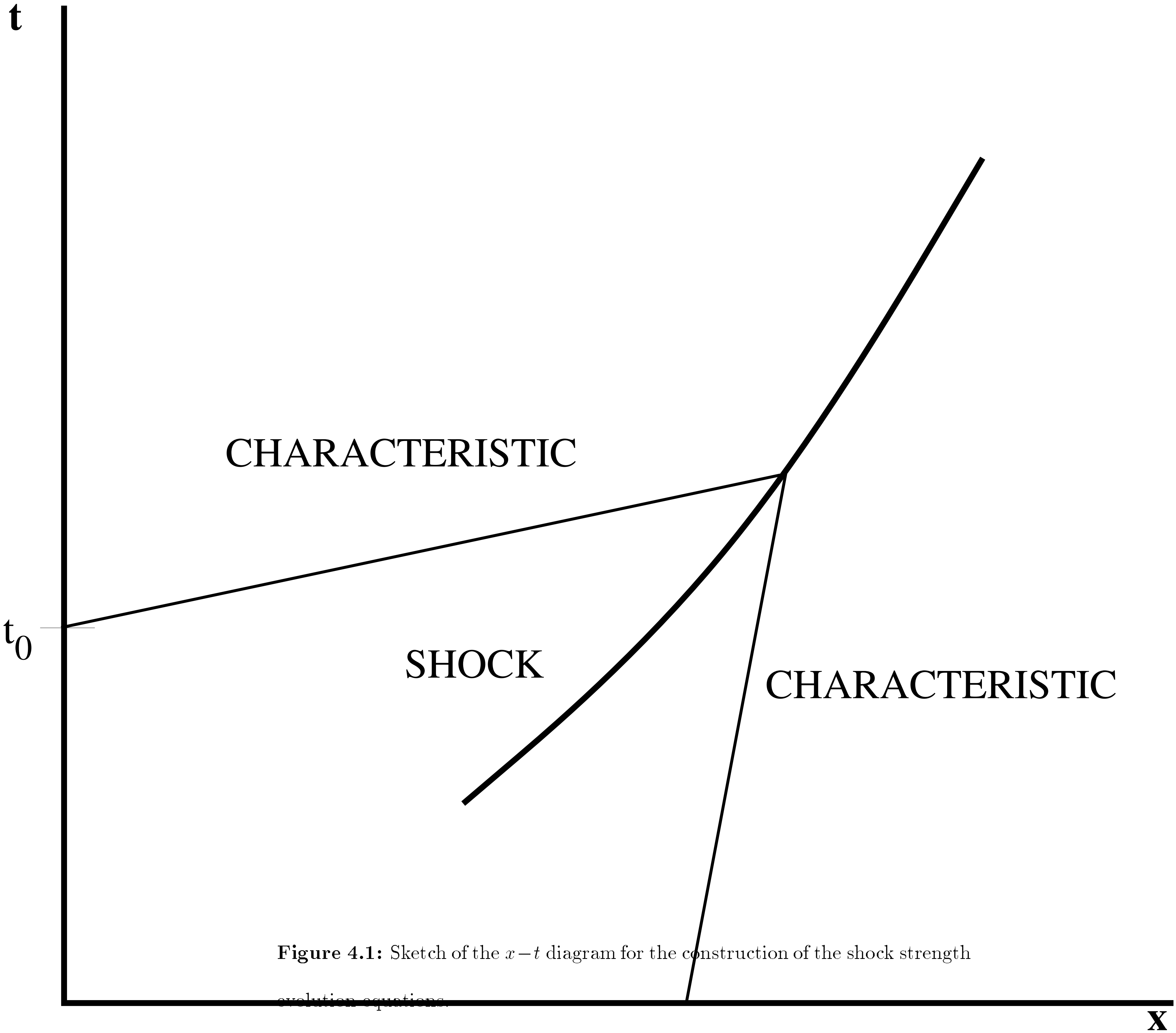

Figure 4.1: Sketch of the $x - t$ diagram for the construction of the shock strength evolution equations.

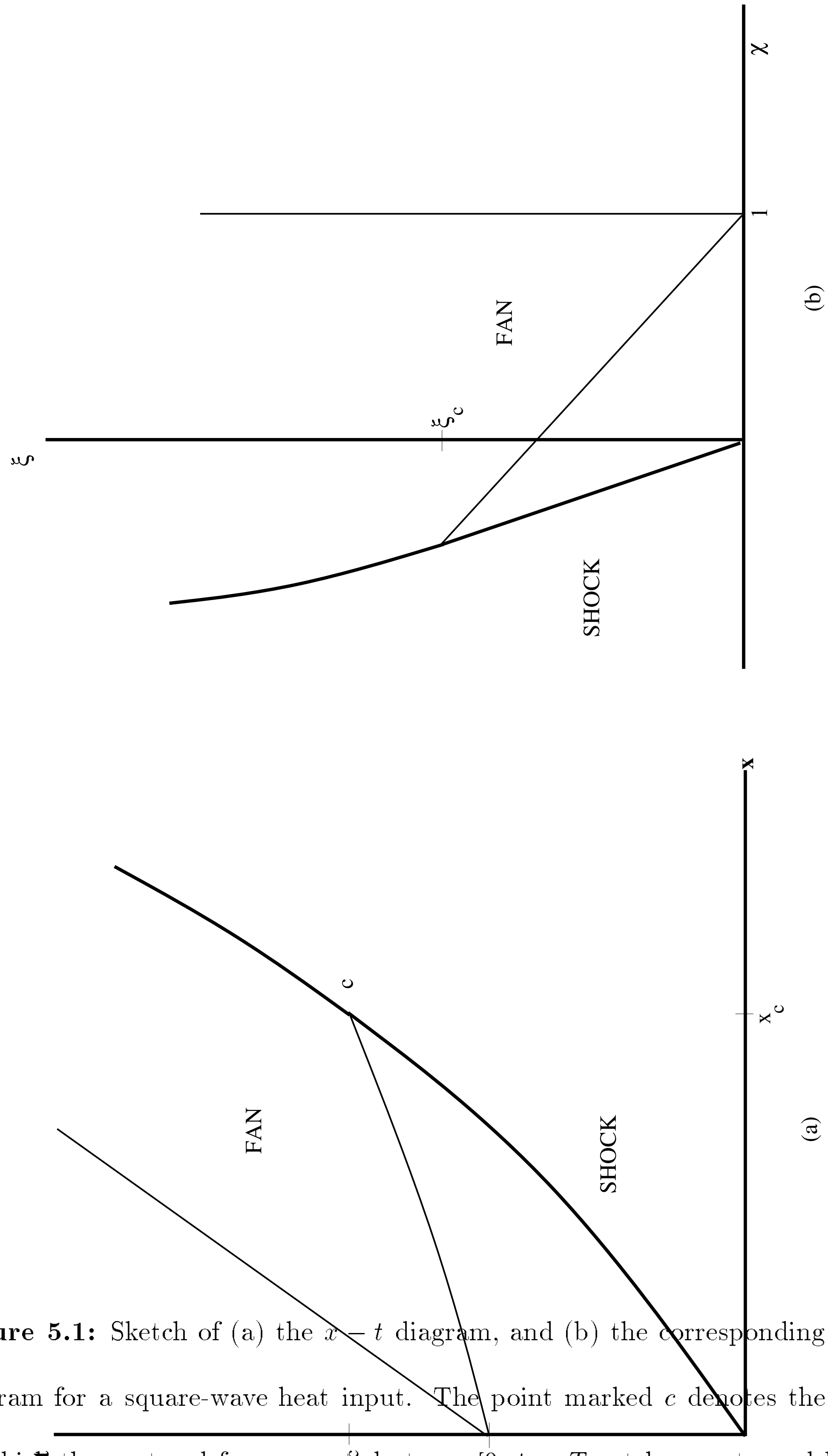

Figure 5.1: Sketch of (a) the $x - t$ diagram, and (b) the corresponding $\xi - \chi$ diagram for a square-wave heat input. The point marked c denotes the point at which the centered fan generated at $x = 0$, $t = T$ catches up to and begins interacting with the shock.

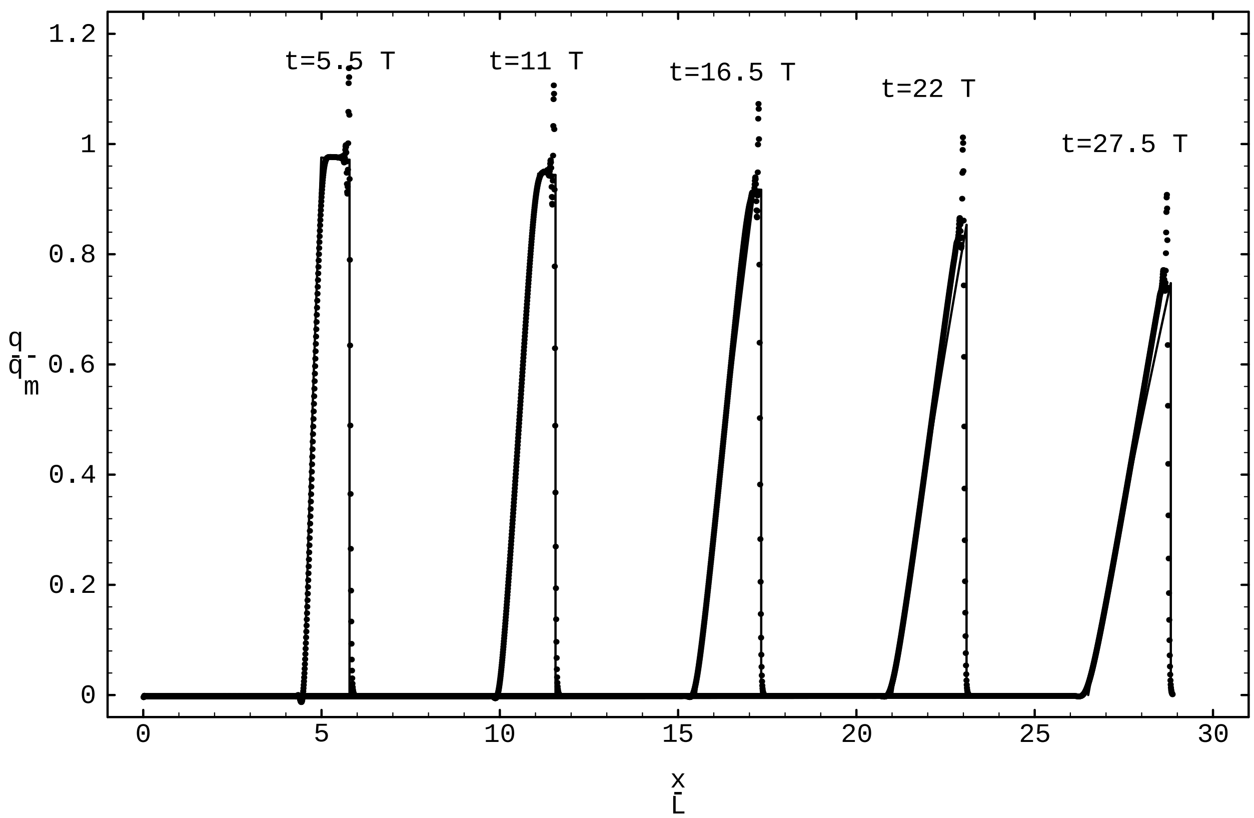

Figure 5.2: Plot of evolution of a square-wave heat input at various scaled times. Solid lines denote the weak-shock solutions developed here and the dots denote numerical solutions to the exact Maxwell-Cattaneo equations (3.1). The parameters chosen were $\epsilon|\Gamma| = 0.1$ and $\delta = 0.01$.

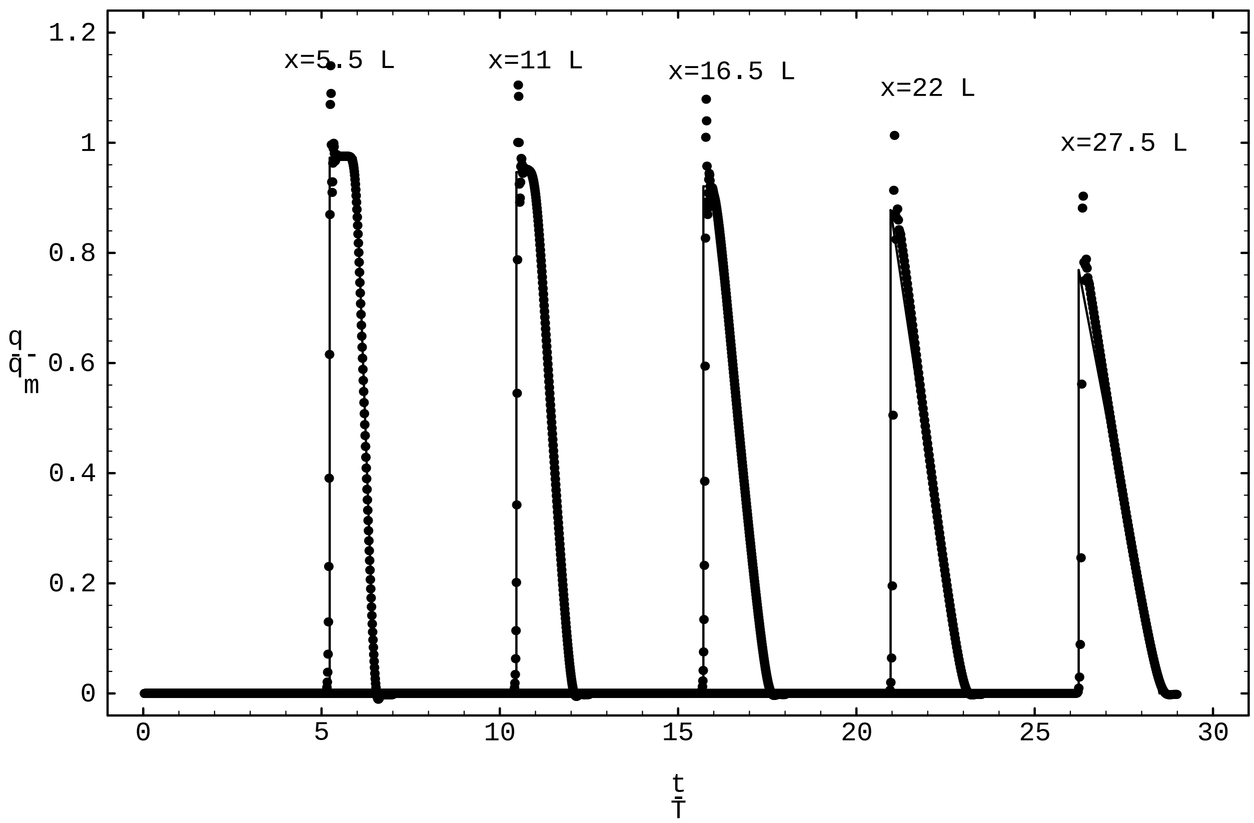

Figure 5.3: Plot of the time signatures for a square-wave heat input computed at various scaled x locations. Solid lines denote the weak-shock solutions and the dots denote numerical solutions to (3.1). The physical parameters are identical to those of Figure 5.2.

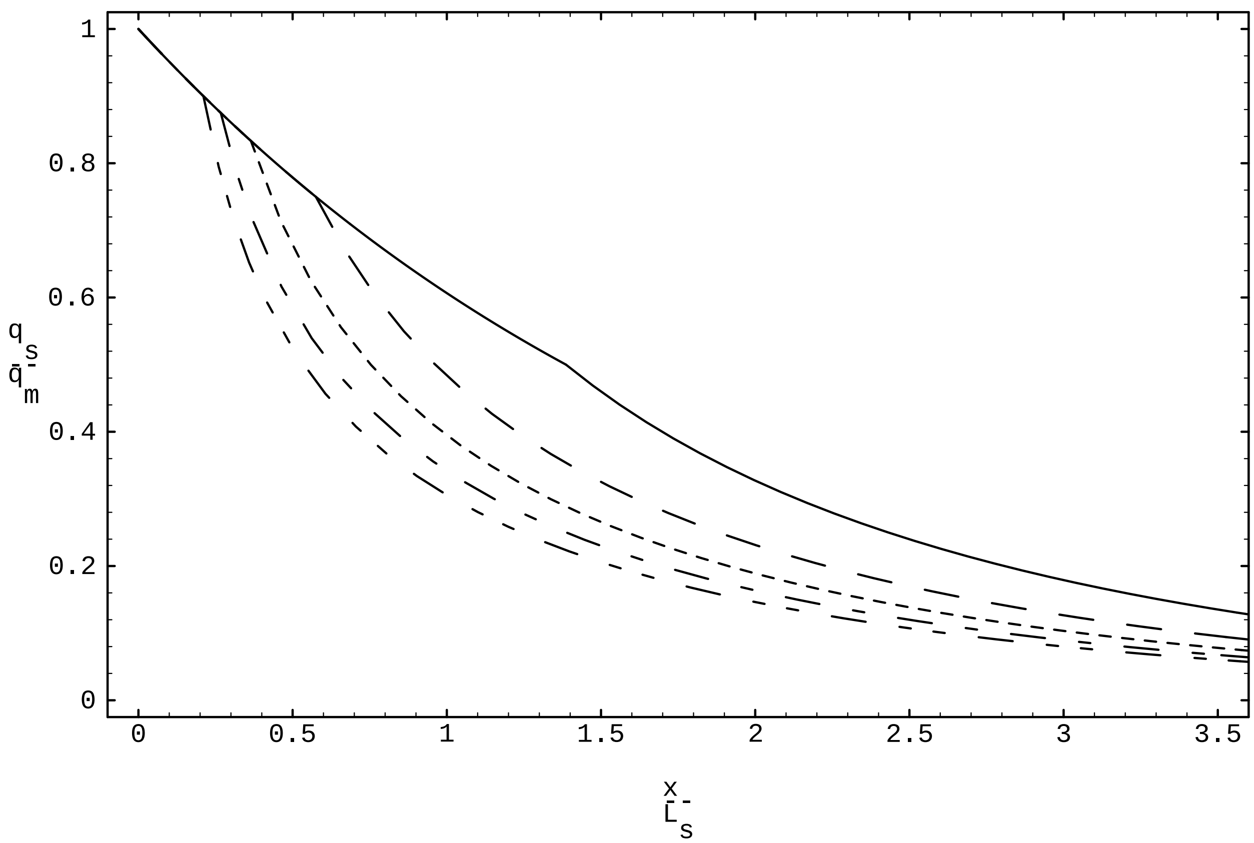

Figure 5.4: Variation of the shock strength as a function of scaled propagation distance for the square-wave heat input. The solid line denotes $B_c = 2$, ________ denotes $B_c = 4$, ________ denotes $B_c = 6$, ________ $B_c = 8$, and ________ denotes $B_c = 10$.

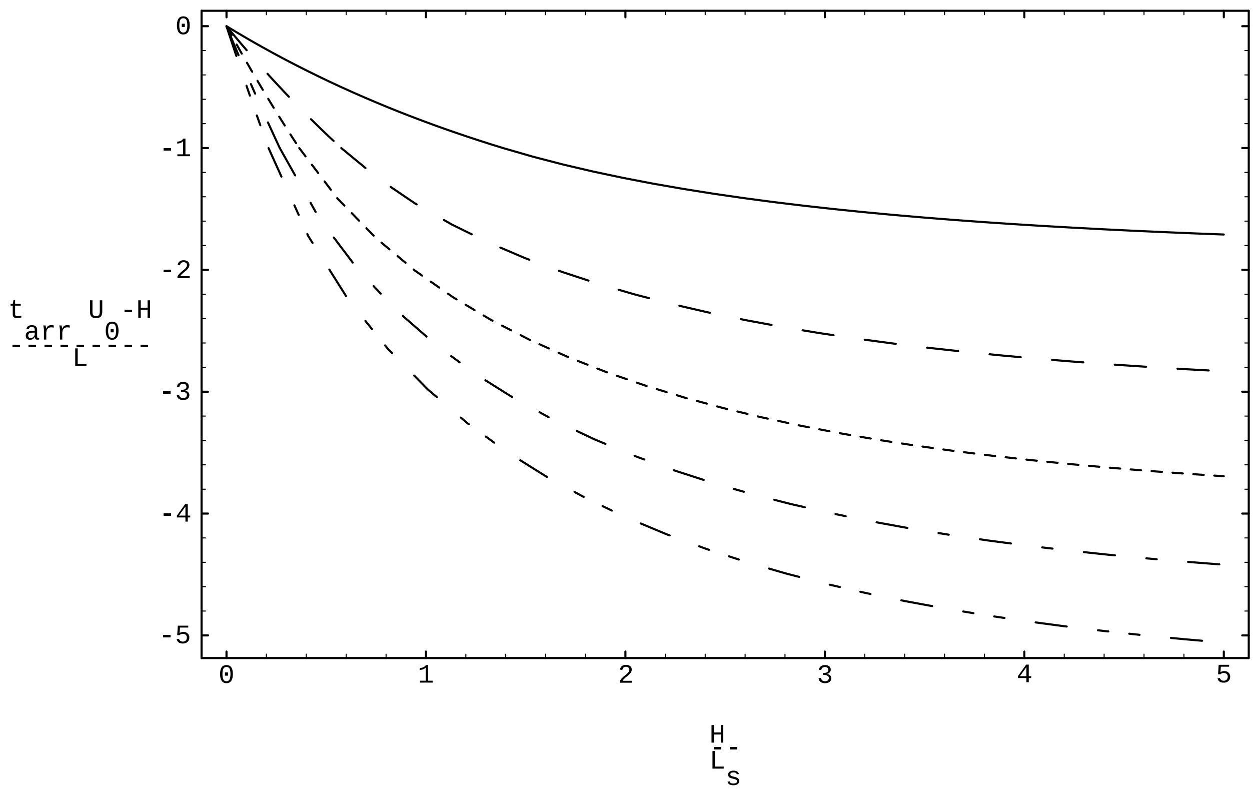

Figure 5.5: Variation of scaled arrival times (t_{arr}) at $x = H$ for the square-wave heat input. Each line type corresponds to the same value of B_c as indicated in Figure 5.4.

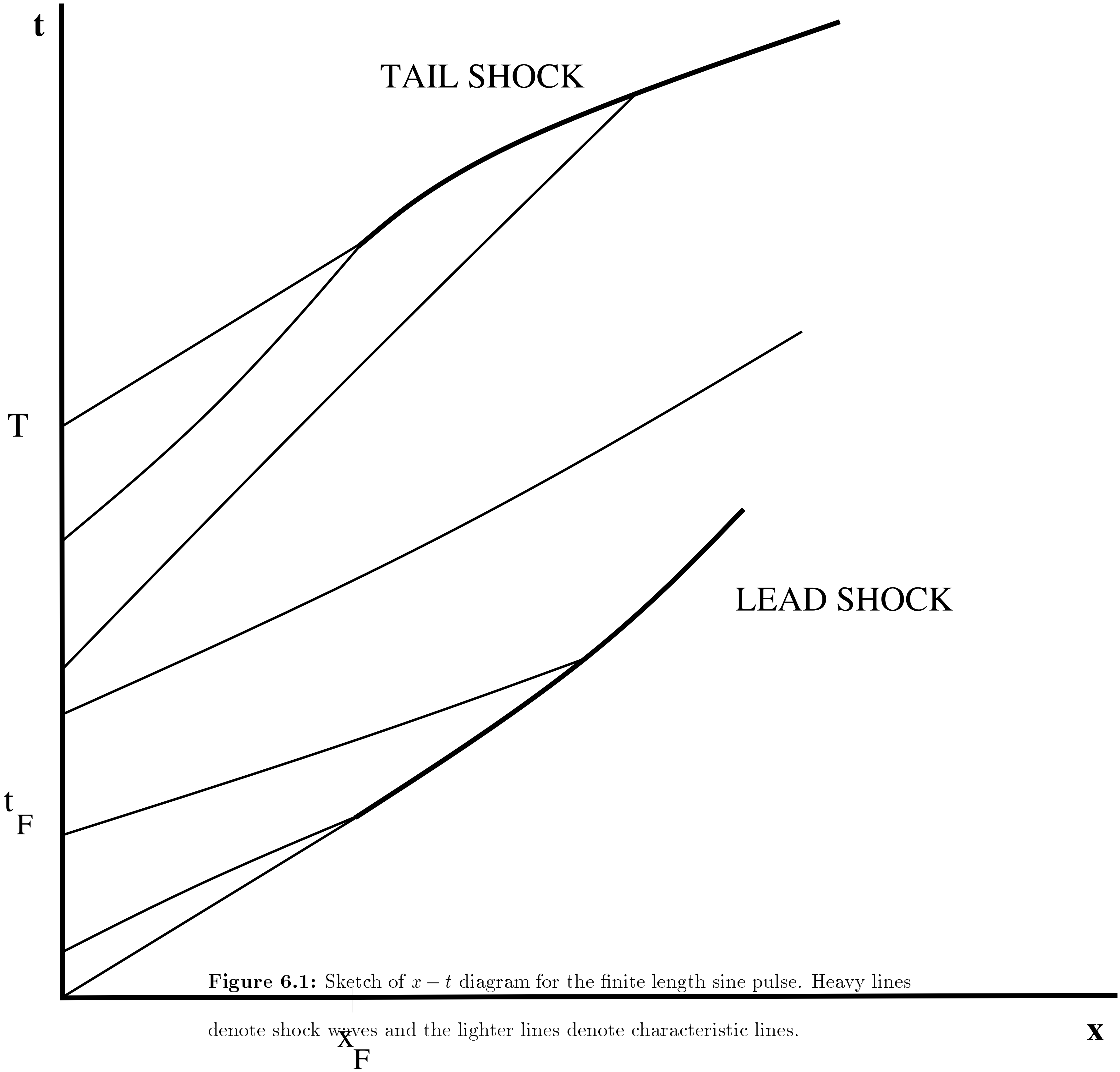

Figure 6.1: Sketch of $x - t$ diagram for the finite length sine pulse. Heavy lines denote shock waves and the lighter lines denote characteristic lines.

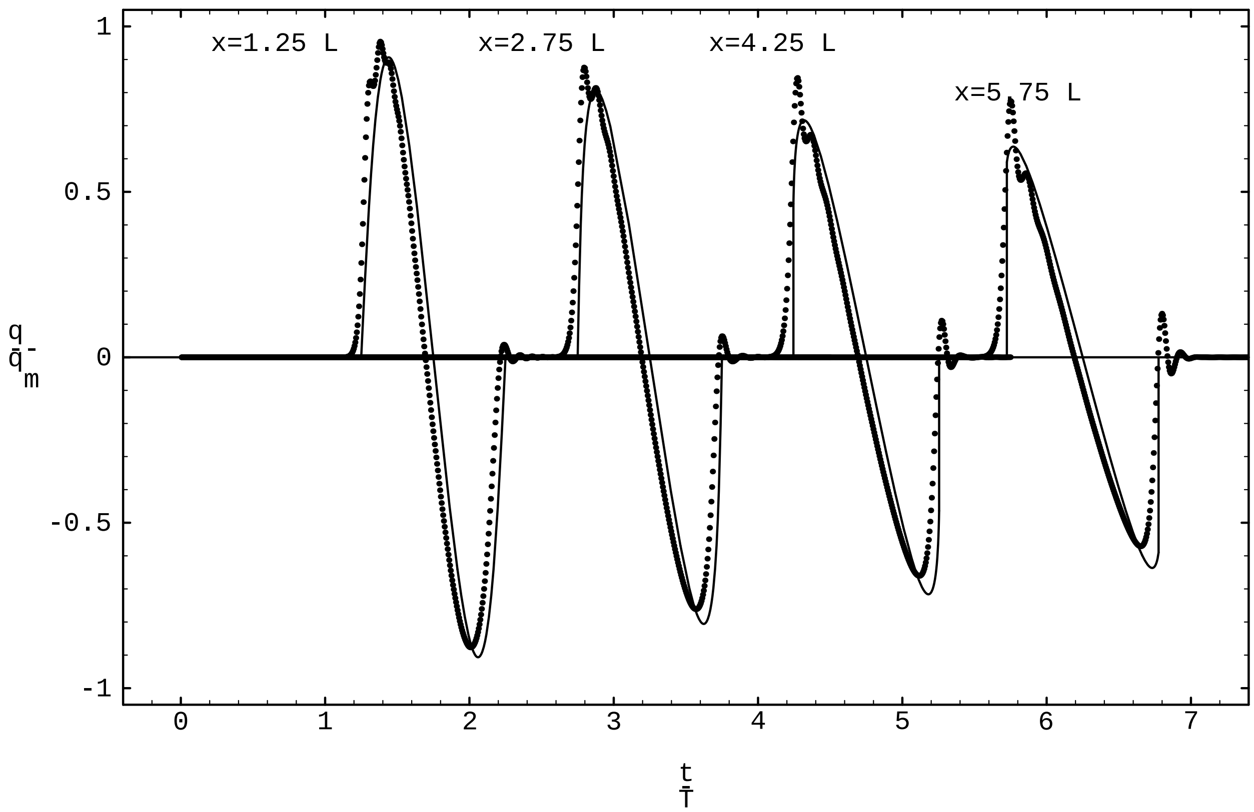

Figure 6.2: Computed time signatures at various x locations for the finite length sine pulse having $\Gamma > 0$. The solid lines denote the weak-shock solutions and the dots denote numerically generated solutions to (3.1). The values of $\epsilon|\Gamma|$ and δ were $1/20$ and $\pi/20$, respectively.

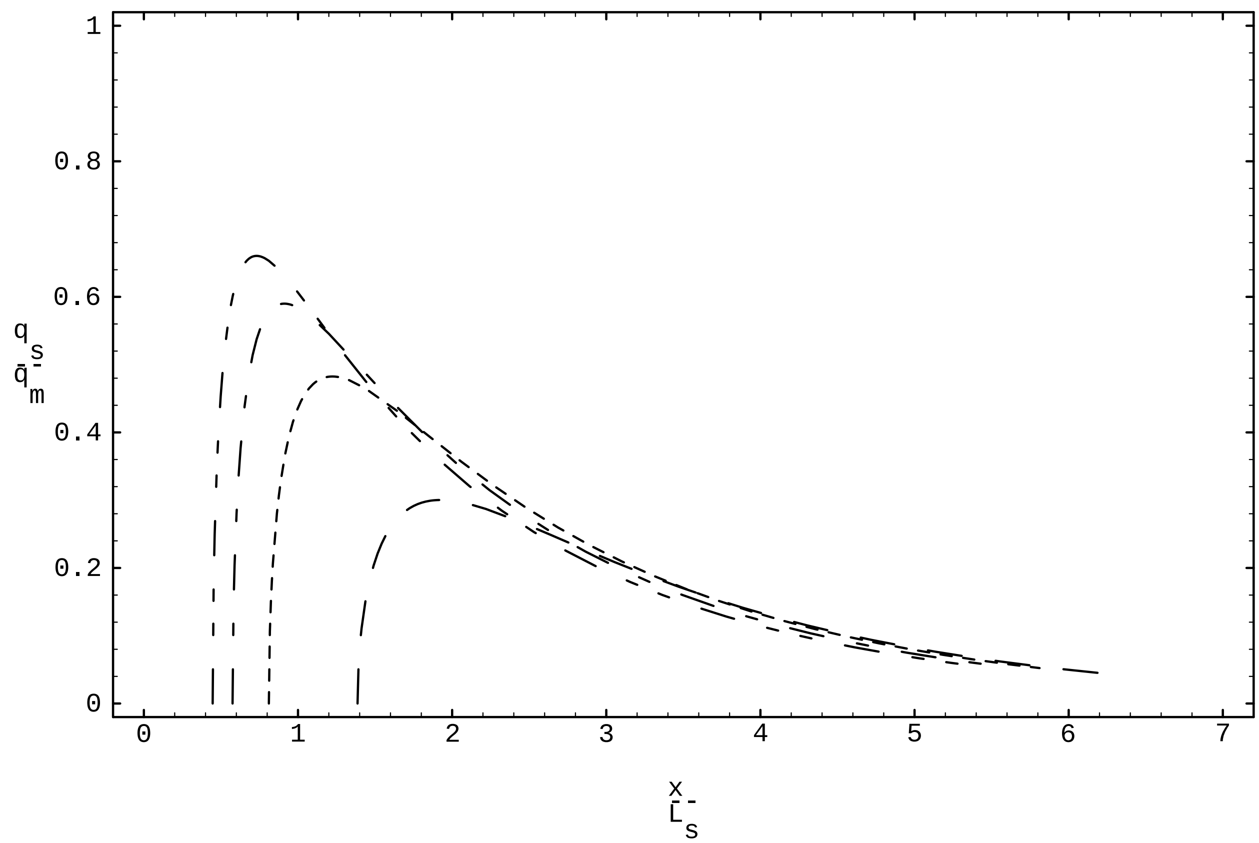

Figure 6.3: Variation of the lead shock strength as a function of scaled propagation distance. The line _______ denotes $B_F = 2$, _______ denotes $B_F = 3$, _______ denotes $B_F = 4$, _______ denotes $B_F = 5$.

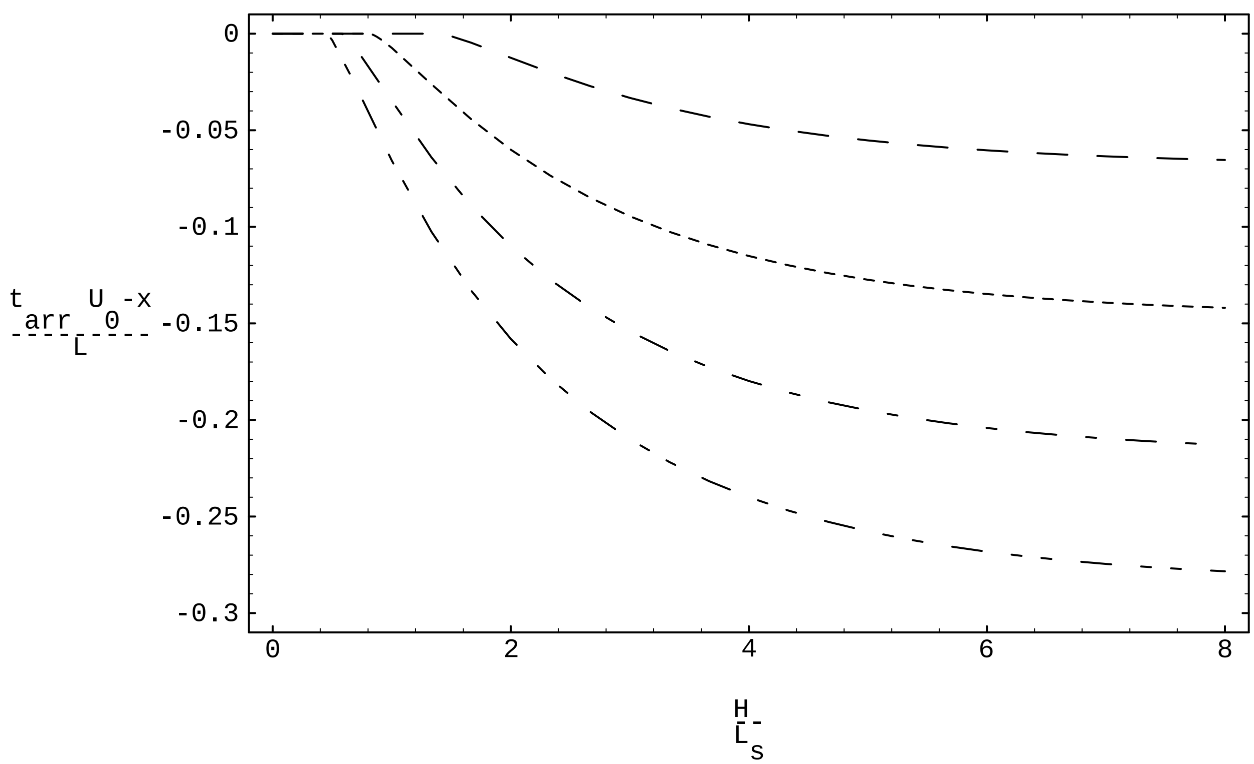

Figure 6.4: Variation of scaled arrival times (t_{arr}) at $x = H$. Each line type corresponds to the same value of B_F as indicated in Figure 6.3.

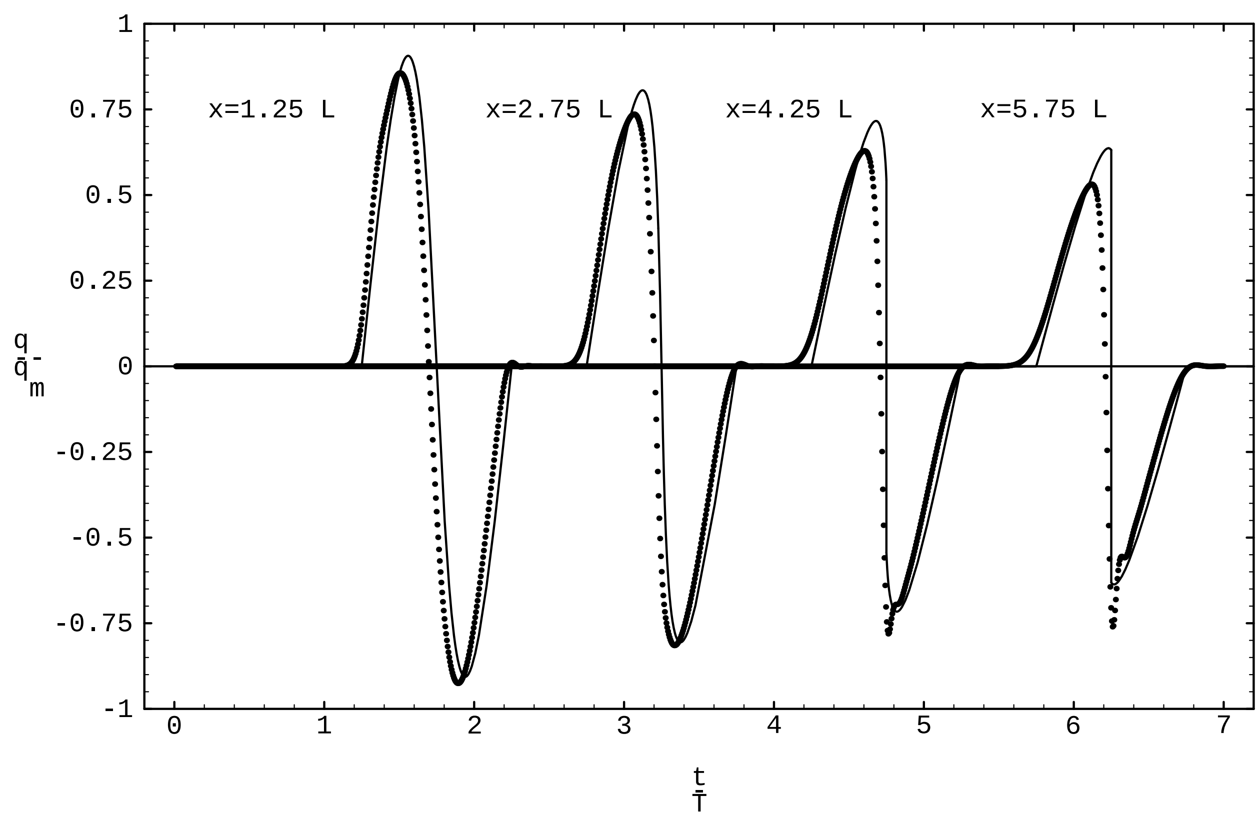

Figure 6.5: Computed time signatures at various locations for the finite length sine pulse having $\Gamma < 0$. The solid lines denote the weak-shock solutions and the dots denote numerically generated solutions to (3.1). The values of $\epsilon|\Gamma|$ and δ are identical to those of Figure 6.2.

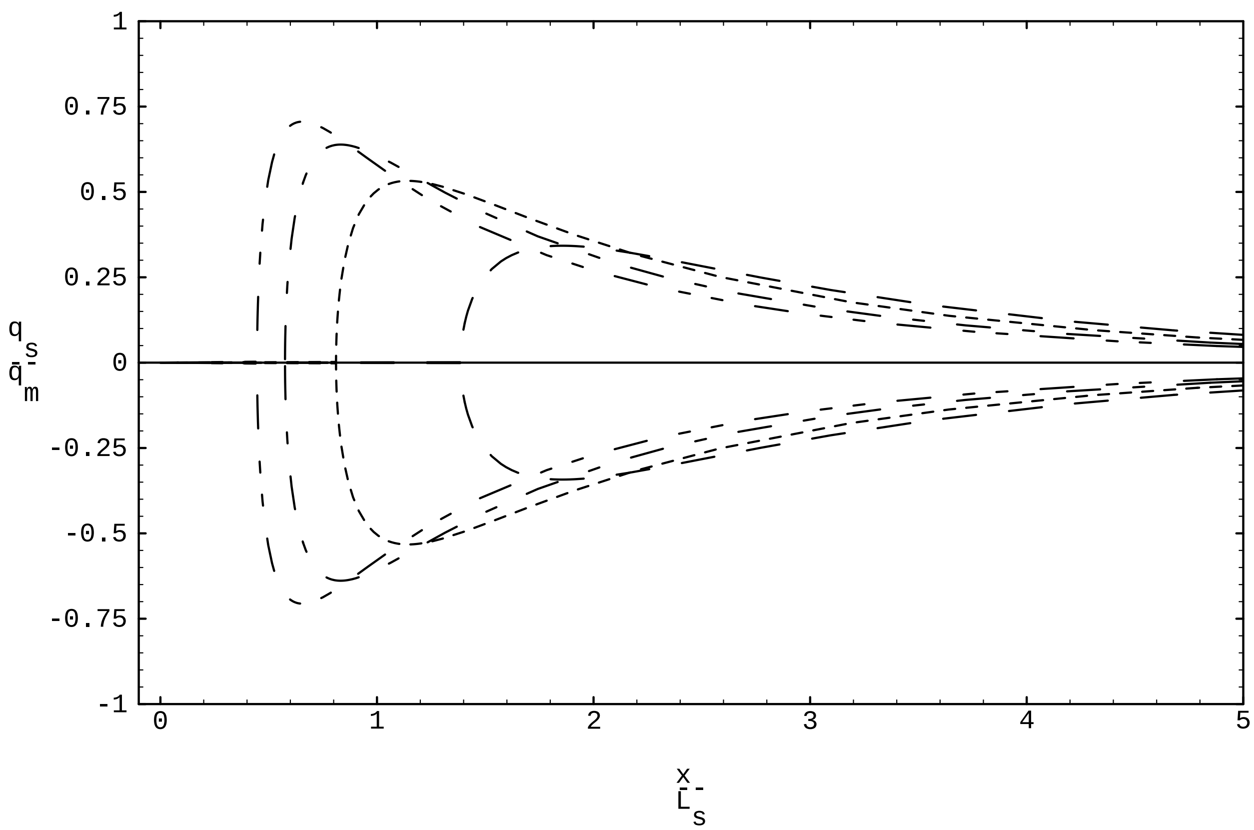

Figure 6.6: Variation of the values of q immediately ahead of and behind the temperature-lowering shock as a function of scaled proportion distance for the finite length sine wave having $\Gamma < 0$. Each line type corresponds to the same value of B_F as indicated in Figure 6.3.